International Journal of Solids and Structures 46 (2009) 507–526

Contents lists available at ScienceDirect

International Journal of Solids and Structures

journal homepage: www.elsevier.com/locate/ijsolstr

Porous materials with two populations of voids under internal pressure: II. Growth and coalescence of voids

Pierre-Guy Vincent [a,b], Yann Monerie [a,c], Pierre Suquet [b,*]

[a] Institut de Radioprotection et de Sûreté Nucléaire, B.P. 3, 13115 Saint-Paul-lez-Durance Cedex, France
[b] Laboratoire de Mécanique et d'Acoustique, 31 Chemin Joseph Aiguier, 13402 Marseille Cedex 20, France
[c] Laboratoire de Micromécanique et d'Intégrité des Structures, IRSN-CNRS-UMII, B.P. 3, 13115 Saint-Paul-lez-Durance Cedex, France

ARTICLE INFO

Article history:
Received 29 May 2008
Received in revised form 4 September 2008
Available online 12 September 2008

Keywords:
Damage
Plasticity
Micromechanics
Void coalescence

ABSTRACT

This study is devoted to the mechanical behaviour of polycrystalline materials with two populations of voids, small spherical voids located inside the grains and larger spheroidal voids located at the grain boundaries. In part I of the work, instantaneous effective stress–strain relations were derived for fixed microstructure. In this second part, the evolution of the microstructure is addressed. Differential equations governing the evolution of the microstructural parameters in terms of the applied loading are derived and their integration in time is discussed. Void growth results in a global softening of the stress–strain response of the material. A simple model for the prediction of void coalescence is proposed which can serve to predict the overall ductility of polycrystalline porous materials under the combined action of thermal dilatation and internal pressure in the voids.

1. Introduction

This study, started in a companion paper (Vincent et al., 2008), is devoted to the mechanical behaviour of uranium oxide (UO_2), a polycrystalline material where, under irradiation, two populations of voids can be observed, small spherical voids in the interior of the grains and larger spheroidal voids at the grain boundaries (see Fig. 6). Under accident condition, the temperature in the material increases suddenly, causing a thermal dilatation of the material and a sudden raise of the pressure of the fission gases in the voids under which the voids can grow and coalesce to form a macro-crack.

In this paper, we continue the derivation of constitutive relations for porous materials containing two populations of voids of different sizes. In part I of this work (Vincent et al., 2008), *instantaneous* constitutive relations were obtained (the terminology is borrowed from Ponte Castañeda and Zaidman (1996)). By instantaneous it is meant that these effective relations between the overall stress and the overall strain-rate are established by considering that the microstructure of the material is fixed. In this second part, the evolution of the microstructure is addressed. This requires first to identify a set of variables characterizing the microstructure to a good degree of accuracy. For the specific problem under consideration where the loading has no preferential direction, simplifying assumptions described in Section 2.1 allow us to reduce the microstructural variables to only three variables, the local volume fraction f_b of the small spherical voids, the volume fraction f_e of the spheroidal intergranular voids and the aspect ratio w of the spheroidal voids. Evolution equations for these variables are given in Section 2.2. The full set of constitutive relations is given in Section 3 where their integration in time is discussed. The predictions of the model are discussed in Section 4. As expected the damage evolution results in a softening of the overall stress–strain curves predicted by the model. However, these curves do not show any sudden drop in the stress which could

* Corresponding author. Tel.: +33 4 91 16 42 08; fax: +33 4 91 16 44 81.
E-mail addresses: pierre-guy.vincent@irsn.fr (P.-G. Vincent), yann.monerie@irsn.fr (Y. Monerie), suquet@lma.cnrs-mrs.fr (P. Suquet).

0020-7683/$ - see front matter © 2008 Elsevier Ltd. All rights reserved.
doi:10.1016/j.ijsolstr.2008.09.004

be interpreted as void coalescence or macroscopic failure. Coalescence of voids is a localized phenomenon where void-to-void interaction plays a crucial role which cannot be captured without information about the arrangement of the intergranular voids. This additional information is introduced in Section 5 where a simple analysis is proposed to predict the type of failure (transgranular or intergranular) and the strain at failure of a biporous material with a specific microstructure.

2. Microstructure evolution

2.1. Microstructural variables

The microstructural variables describe the shape and distribution of the two populations of voids. In full generality the microstructure evolution is a complex problem. For instance, ellipsoidal voids with different orientations should be considered as different phases. Similarly, because of the heterogeneity of the intragranular strain field, the growth of the secondary voids (small, spherical voids) is likely to be inhomogeneous. Therefore, the porosity f_b of the small voids should be considered as a field at the mesoscopic scale and the different values of this field at different points in a mesoscopic volume element should appear in the microstructural (or mesostructural) variables of the model. Accounting for all the details of this heterogeneity would result in a formidably complicated model. Therefore, simplifying assumptions are introduced to keep the size of the model compatible with its implementation in a structural code. These simplifications are motivated by the specific application which we have in mind as described in the introduction of the first part of this study, namely a sudden increase in pressure inside the voids and an overall hydrostatic deformation of the volume element. Under such loading conditions, it is in particular expected that no direction plays a preferential role so that it is not necessary to account for different orientations in the intergranular voids. Clearly, the validity of these assumptions is limited to the problem at hand and should be revisited for a different problem. These assumptions read as follows:

H1: *The secondary voids* (*small intragranular voids*) *remain spherical in shape and their volume fraction is described by a single variable* $f_b(t)$.
H2: *The primary voids* (*large spheroidal intergranular voids*) *remain spheroidal in shape. All voids, even with different orientations are assumed to have the same aspect ratio* $w(t)$. *Their overall volume fraction is described by a single variable* $f_e(t)$.
H3: *The distance between the focii of each individual ellipsoid remains fixed during the evolution.*
H4: *The evolution of the microstructural variables* $f_b(t),\ f_e(t),\ w(t)$ *is only due to plasticity effects*. In other words these variables are not affected by the overall elastic deformation.

Comments:

(1) As a consequence of assumptions (H1) and (H2), the whole microstructure is characterized by only three time-dependent variables, $f_b(t),\ f_e(t)$ and $w(t)$. The merit of this minimalist description of the microstructure is that it can be easily implemented in a standard finite element package. In a more general description, which would probably be required to model the deformation of biporous materials under general loading conditions, ellipsoids with different orientation should be considered as different phases with their own volume fraction and their own aspect ratio for all possible orientations. This would lead to a model with a large number of microstructural variables, a situation similar to that encountered in the micromechanical modelling of texture evolution in polycrystals. This direction is not pursued here.
(2) Under the simplifying assumption (H2) according to which all ellipsoids are described by a single aspect ratio, there are several possible approximate ways to obtain an evolution equation for w. The idea behind assumption (H3) is that under internal pressure a flat ellipsoid should become more spherical as its volume increases. This is ensured by assumption (H3) as one can see by considering a family of confocal ellipsoids starting from a penny-shaped crack. Since the focii of the ellipsoid remain fixed during the deformation, the various stages of the deformation of the ellipsoid belong to the family of ellipsoids parameterized by a scalar parameter λ as described in Appendix B of the first part of this study. The corresponding ellipsoids tend to become spherical when their volume increases, or equivalently when the parameter λ increases.

2.2. Evolution of the microstructural variables

2.2.1. Evolution of the volume fraction f_b of the small spherical voids

Classically, a first evolution equation is provided by the mass balance equation at the macroscopic scale:

$$\dot{f} = (1-f)\mathrm{tr}\dot{\boldsymbol{E}}, \tag{1}$$

where f denotes the total porosity which can be expressed in terms of the intragranular porosity f_b and of the intergranular porosity f_e as (see relation (1) of Vincent et al. (2008))

$$f = f_e + f_b(1-f_e).$$

The mass balance equation can be alternatively written as

$$\dot{f}_b = (1-f_b)\left(\operatorname{tr}\dot{\boldsymbol{E}} - \frac{\dot{f}_e}{1-f_e}\right). \tag{2}$$

2.2.2. Evolution of the volume fraction f_e of the large ellipsoidal voids

Consider a mesoscopic volume element containing ellipsoidal voids occupying a domain ω_e possibly composed of several different voids with different orientations. Recall that the void volume fraction of the ellipsoidal voids is $f_e = |\,\omega_e\,| / |\,V\,|$. Taking the logarithmic derivative of this relation yields

$$\frac{\dot{f}_e}{f_e} = \frac{|\,\dot{\omega_e}\,|}{|\,\omega_e\,|} - \frac{|\,\dot{V}\,|}{|\,V\,|} = \langle \operatorname{tr}\dot{\boldsymbol{\varepsilon}}\rangle_{\omega_e} - \operatorname{tr}\dot{\boldsymbol{E}}, \quad \text{i.e., } \dot{f}_e = f_e(\langle \operatorname{tr}\dot{\boldsymbol{\varepsilon}}\rangle_{\omega_e} - \operatorname{tr}\dot{\boldsymbol{E}}).$$

The relation between $\langle \operatorname{tr}\dot{\boldsymbol{\varepsilon}}\rangle_{\omega_e}$ and $\operatorname{tr}\dot{\boldsymbol{E}}$ depends on the micromechanical model used in the analysis of the instantaneous effective properties. In the present paper, we make use of the N-phase modified secant method developed in the first part of this work (Vincent et al., 2008). First, the population of randomly oriented spheroidal voids dispersed in a Gurson matrix is replaced by a distribution of spherical voids. Second, the matrix is divided into N concentric phases. Third, the modified secant method is used to determine the local strain-rate fields and the effective properties. In particular, the change in volume of the ellipsoidal voids $\langle \operatorname{tr}\dot{\boldsymbol{\varepsilon}}\rangle_{\omega_e}$ can be related to the overall change in volume $\operatorname{tr}\dot{\boldsymbol{E}}$ and to the pressure difference $p^* = p_e - p_b$ by

$$\langle \operatorname{tr}\dot{\boldsymbol{\varepsilon}}\rangle_{\omega_e} = \boldsymbol{i} : \left(\boldsymbol{A}_e^{(1)} : \dot{\boldsymbol{E}} + \boldsymbol{a}_e^{(1)}\right) = \frac{1}{f_e}\left(b_e \operatorname{tr}\dot{\boldsymbol{E}} + \frac{p^*}{M_e}\right), \quad p^* = p_e - p_b, \tag{3}$$

where $\boldsymbol{A}_e^{(1)}$ denotes the elastic localization tensor in the ellipsoidal voids (in the absence of pressure), and $\boldsymbol{a}_e^{(1)}$ is the average strain-rate in the voids due to the internal pressure only (in the absence of overall strain-rate), both being delivered by the N-phase model (see Vincent et al., 2008 for details). The final form of the evolution equation for f_e is

$$\dot{f}_e = (b_e - f_e)\operatorname{tr}\dot{\boldsymbol{E}} + \frac{p^*}{M_e}. \tag{4}$$

Let us recall that the Biot moduli b_e and M_e in the linear comparison voided material containing ellipsoidal voids are related to the Biot moduli b_s and M_s in the N-phase comparison voided material with spherical voids by means of the equivalent porosity f_s^k introduced in the first part of this study, through

$$b_e = b_s(f_s^k), \quad M_e = M_s(f_s^k). \tag{5}$$

For simplicity, the index s will be omitted in what follows and b and M will refer to the Biot moduli whose expressions can be found in Appendix C of the first part of this study.

2.3. Evolution of the aspect ratio of the large ellipsoidal voids

All ellipsoidal voids are self-similar and their evolution is assumed to be self-similar as well. It is therefore sufficient to consider a single void. Let a_1 and b_1 denote the minor semi-axis and major semi-axis of one of the ellipsoidal voids. The focii of all ellipsoids are located on a circle with radius c given by

$$c = \sqrt{b_1^2 - a_1^2},$$

and since c remains constant according to assumption (H3), one has

$$\dot{c} = 0 \quad \text{therefore} \quad \frac{\dot{b}_1}{b_1} = w^2\frac{\dot{a}_1}{a_1}.$$

This relation yields an evolution equation for the void aspect ratio w:

$$w = \frac{a_1}{b_1}, \quad \dot{w} = w\left(\frac{\dot{a}_1}{a_1} - \frac{\dot{b}_1}{b_1}\right) = w\frac{\dot{a}_1}{a_1}(1-w^2). \tag{6}$$

The relative change in volume of the population of voids is the same as that of a single ellipsoid:

$$\langle \operatorname{tr}\dot{\boldsymbol{\varepsilon}}\rangle_{\omega_e} = \frac{|\,\dot{\omega_e}\,|}{|\,\omega_e\,|} = \frac{\dot{a}_1}{a_1} + \frac{2\dot{b}_1}{b_1} = \frac{\dot{a}_1}{a_1}(1+2w^2).$$

This last relation, together with (3) and (6), yields the following evolution equation for w:

$$\dot{w} = \frac{1}{f_e}\frac{w(1-w^2)}{1+2w^2}\left(b_e \operatorname{tr}\dot{\boldsymbol{E}} + \frac{p^*}{M_e}\right). \tag{7}$$

3. Effective constitutive relations and their integration in time

The final model consists of two sets of equations:

(1) The instantaneous effective equations derived in Vincent et al., 2008 relating the overall stress $\boldsymbol{\Sigma}$ and the overall deformation $\boldsymbol{E}$ and its time-derivative. In order to account for elasticity effects which were neglected in Vincent et al., 2008, a slight modification has to be introduced in these equations by splitting the total deformation into an elastic and a plastic part $\boldsymbol{E} = \boldsymbol{E}^{\mathrm{e}} + \boldsymbol{E}^{\mathrm{p}}$. The poro-elastic relations derived in Section 3 of Vincent et al., 2008 relate the overall stress and the elastic deformation $\boldsymbol{E}^{\mathrm{e}} = \boldsymbol{E} - \boldsymbol{E}^{\mathrm{p}}$ through

$$\boldsymbol{\Sigma} = \mathbf{C}_2^{\mathrm{hom}} : \boldsymbol{E}^{\mathrm{e}} - [b_2(p_e - b_1 p_b) + b_1 p_b]\boldsymbol{i}, \tag{8}$$

In the above relation, b_1 and b_2 stand for the Biot coefficients of the porous material at the mesoscopic and macroscopic scale, respectively (Vincent et al., 2008), and should not be confused with the major axis of the outer and inner ellipsoids.

The evolution of the plastic strain $\boldsymbol{E}^{\mathrm{p}}$ is governed by the instantaneous constitutive relations established in Vincent et al., 2008. An (instantaneous) effective plasticity domain P^{hom} has been introduced which is such that

$$\begin{aligned} &\boldsymbol{\Sigma} \in P^{\mathrm{hom}} \\ &\quad \text{when } \boldsymbol{\Sigma} \text{ is in the interior of } P^{\mathrm{hom}} : \ \dot{\boldsymbol{E}}^{\mathrm{p}} = \mathbf{0}, \\ &\quad \text{when } \boldsymbol{\Sigma} \text{ is on the boundary of } P^{\mathrm{hom}} : \ \boldsymbol{\Sigma} = \mathfrak{f}(\dot{\boldsymbol{E}}^{\mathrm{p}}, f_b, f_e, w, p_b, p_e), \end{aligned} \tag{9}$$

where $\mathfrak{f}$ is given by the N-phase model of Vincent et al., 2008. Note that, for comparison with Vincent et al., 2008 where elastic effects were neglected, the stress is related here to the plastic strain-rate $\dot{\boldsymbol{E}}^{\mathrm{p}}$ and not to the total strain-rate $\dot{\boldsymbol{E}}$.

(2) The evolution equations for the microstructural parameters $f_b(t)$, $f_e(t)$ and $w(t)$ derived in Section 2.2. According to assumption (H4) the overall elastic deformation does not contribute to the change in the microstructural variables and, again, $\dot{\boldsymbol{E}}$ should be replaced by $\dot{\boldsymbol{E}}^{\mathrm{p}}$ in (2), (4) and (7).

The constitutive relations describing the evolution of the plastic strain and of the microstructure, assuming that the strains remain infinitesimal, read as

$$\begin{aligned} &\boldsymbol{\Sigma} = \mathbf{C}_2^{\mathrm{hom}} : (\boldsymbol{E} - \boldsymbol{E}^{\mathrm{p}}) - [b_2(p_e - b_1 p_b) + b_1 p_b]\boldsymbol{i}, \\ &\boldsymbol{\Sigma} \in P^{\mathrm{hom}} \\ &\quad \text{when } \boldsymbol{\Sigma} \text{ is in the interior of } P^{\mathrm{hom}} : \ \dot{\boldsymbol{E}}^{\mathrm{p}} = \mathbf{0}, \\ &\quad \text{when } \boldsymbol{\Sigma} \text{ is on the boundary of } P^{\mathrm{hom}} : \ \boldsymbol{\Sigma} = \mathfrak{f}(\dot{\boldsymbol{E}}^{\mathrm{p}}, f_b, f_e, w, p_b, p_e), \end{aligned} \tag{10}$$

$$\begin{aligned} \dot{f}_b &= \frac{1 - f_b}{1 - f_e}\left((1 - b_e)\mathrm{tr}\dot{\boldsymbol{E}}^{\mathrm{p}} - \frac{p_e - p_b}{M_e}\right) \quad \text{i.e. } \dot{f}_b \equiv \mathfrak{g}_1(\dot{\boldsymbol{E}}^{\mathrm{p}}, f_b, f_e, w, p_b, p_e), \\ \dot{f}_e &= (b_e - f_e)\mathrm{tr}\dot{\boldsymbol{E}}^{\mathrm{p}} + \frac{p_e - p_b}{M_e} \quad \text{i.e. } \dot{f}_e \equiv \mathfrak{g}_2(\dot{\boldsymbol{E}}^{\mathrm{p}}, f_b, f_e, w, p_b, p_e), \\ \dot{w} &= \frac{1}{f_e}\frac{w(1 - w^2)}{1 + 2w^2}\left(b_e \mathrm{tr}\dot{\boldsymbol{E}}^{\mathrm{p}} + \frac{p_e - p_b}{M_e}\right) \quad \text{i.e. } \dot{w} \equiv \mathfrak{g}_3(\dot{\boldsymbol{E}}^{\mathrm{p}}, f_b, f_e, w, p_b, p_e). \end{aligned} \tag{11}$$

The above system of strongly nonlinear differential equations for the unknowns $\boldsymbol{\Sigma}(t)$, $\dot{\boldsymbol{E}}^{\mathrm{p}}(t)$, $f_b(t)$, $f_e(t)$ and $w(t)$ is solved numerically by means of an implicit Euler scheme which is a generalization of the classical closest-point algorithm in Plasticity (Nguyen, 1977; Simo and Hughes, 1998). The loading parameters $(\boldsymbol{E}(t), p_b(t), p_e(t))$ follow a prescribed path. The initial state of the microstructure is given and this is reflected through initial conditions f_b^0, f_e^0, w^0 for the microstructural parameters. To simplify the integration, the effective poro-elastic characteristics of the voided material $\mathbf{C}_2^{\mathrm{hom}}, b_2, b_1$ are assumed to remain constant in time and are computed once and for all by means of the initial value of the microstructural parameters (in full rigor the elastic characteristics also depend on f_e, f_b, and w but to a much lesser extent than the plastic properties). The first equation in (10) can then be replaced by its incremental version obtained by derivation with respect to time:

$$\dot{\boldsymbol{\Sigma}} = \mathbf{C}_2^{\mathrm{hom}} : (\dot{\boldsymbol{E}} - \dot{\boldsymbol{E}}^{\mathrm{p}}) - [b_2(\dot{p}_e - b_1 \dot{p}_b) + b_1 \dot{p}_b]\boldsymbol{i}. \tag{12}$$

The time interval of study $[0, T]$ is discretized into successive time steps $[t_n, t_{n+1}]$, and the value of a function f at time t_n is denoted by f_n. Assuming that the value at time t_n of all unknowns have been determined at the end of the preceding time-step, new values $(\boldsymbol{E}_{n+1}, (p_b)_{n+1}, (p_e)_{n+1})$ are prescribed to the loading parameters. The unknowns $\boldsymbol{\Sigma}, \dot{\boldsymbol{E}}^{\mathrm{p}}, f_b, f_e, w$ at time t_{n+1} (note that the subscript $n+1$ is omitted to simplify notations) solve a time-discretized version of the equations (10) and (12):

$$\begin{aligned} &\boldsymbol{\Sigma} = \boldsymbol{\Sigma}_n + \mathbf{C}_2^{\mathrm{hom}} : (\Delta\boldsymbol{E} - \Delta t\dot{\boldsymbol{E}}^{\mathrm{p}}) - [b_2\Delta(p_e - b_1 p_b) + b_1 \Delta p_b]\boldsymbol{i} \\ &\boldsymbol{\Sigma} \in P^{\mathrm{hom}}, \\ &\quad \text{when } \boldsymbol{\Sigma} \text{ is in the interior of } P^{\mathrm{hom}} : \ \dot{\boldsymbol{E}}^{\mathrm{p}} = \mathbf{0}, \end{aligned}$$

$$\begin{aligned}
&\text{when } \boldsymbol{\Sigma} \text{ is on the boundary of } P^{\hom}: \ \boldsymbol{\Sigma} = \mathfrak{f}(\dot{\boldsymbol{E}}^{\mathrm{p}}, f_b, f_e, w, (p_b)_{n+1}, (p_e)_{n+1}),\\
&f_b = (f_b)_n + \Delta t \mathfrak{g}_1(\dot{\boldsymbol{E}}^{\mathrm{p}}, f_b, f_e, w, (p_b)_{n+1}, (p_e)_{n+1}),\\
&f_e = (f_e)_n + \Delta t \mathfrak{g}_2(\dot{\boldsymbol{E}}^{\mathrm{p}}, f_b, f_e, w, (p_b)_{n+1}, (p_e)_{n+1}),\\
&w = w_n + \Delta t \mathfrak{g}_3(\dot{\boldsymbol{E}}^{\mathrm{p}}, f_b, f_e, w, (p_b)_{n+1}, (p_e)_{n+1}),
\end{aligned} \tag{13}$$

where $\Delta t = t_{n+1} - t_n$ with similar definitions for $\Delta \boldsymbol{E}$, Δp_b and Δp_e. The *trial stress* $\boldsymbol{\Sigma}^{\mathrm{Trial}}$, which is the purely elastic response of the system under the applied increment of loading, reads as

$$\boldsymbol{\Sigma}^{\mathrm{Trial}} = \boldsymbol{\Sigma}_n + \boldsymbol{C}_2^{\hom} : \Delta \boldsymbol{E} - [b_2 \Delta(p_e - b_1 p_b) + b_1 \Delta p_b]\boldsymbol{i}.$$

Two cases must be considered.

- Either $\boldsymbol{\Sigma}^{\mathrm{Trial}}$ belongs to $P^{\hom}$, in which case the step is purely elastic and

$$\boldsymbol{\Sigma} = \boldsymbol{\Sigma}^{\mathrm{Trial}}, \quad f_b = (f_b)_n, \quad f_e = (f_e)_n, \quad w = w_n.$$

- Or $\boldsymbol{\Sigma}^{\mathrm{Trial}}$ does not belong to $P^{\hom}$, the step is plastic and the stress $\boldsymbol{\Sigma}$ is on the yield surface. The following nonlinear equations has to be solved for $\dot{\boldsymbol{E}}^{\mathrm{p}}, f_b, f_e, w$:

$$\begin{aligned}
&\mathfrak{f}(\dot{\boldsymbol{E}}^{\mathrm{p}}, f_b, f_e, w, (p_b)_{n+1}, (p_e)_{n+1}) = \boldsymbol{\Sigma}^{\mathrm{Trial}} - \Delta t \boldsymbol{C}_2^{\hom} : \dot{\boldsymbol{E}}^{\mathrm{p}},\\
&f_b = (f_b)_n + \Delta t \mathfrak{g}_1(\dot{\boldsymbol{E}}^{\mathrm{p}}, f_b, f_e, w, (p_b)_{n+1}, (p_e)_{n+1}),\\
&f_e = (f_e)_n + \Delta t \mathfrak{g}_2(\dot{\boldsymbol{E}}^{\mathrm{p}}, f_b, f_e, w, (p_b)_{n+1}, (p_e)_{n+1}),\\
&w = w_n + \Delta t \mathfrak{g}_3(\dot{\boldsymbol{E}}^{\mathrm{p}}, f_b, f_e, w, (p_b)_{n+1}, (p_e)_{n+1}).
\end{aligned} \tag{14}$$

This system is solved by means of a Newton–Raphson procedure (where the gradient is computed numerically by a difference quotient). Once the solution $\dot{\boldsymbol{E}}^{\mathrm{p}}, f_b, f_e, w$ is determined, the stress $\boldsymbol{\Sigma}$ is obtained as

$$\boldsymbol{\Sigma} = \mathfrak{f}(\dot{\boldsymbol{E}}^{\mathrm{p}}, f_b, f_e, w, (p_b)_{n+1}, (p_e)_{n+1}).$$

Remark. The instantaneous plasticity domain $P^{\hom}$ is only defined implicitly by the N-phase model and the verification of the condition $\boldsymbol{\Sigma}^{\mathrm{Trial}} \in P^{\hom}$ is not straightforward. In a first step an interior point of $P^{\hom}$ is determined. This can be done, among other possibilities, by computing the stresses Σ_m^+ and Σ_m^- corresponding, respectively, to positive and negative hydrostatic $\dot{\boldsymbol{E}}^{\mathrm{p}}$ in the relation (9) (see Fig. 1). The stress $\overline{\boldsymbol{\Sigma}} = 1/2(\Sigma_m^+ + \Sigma_m^-)\boldsymbol{i}$ is in the interior of $P^{\hom}$. Then consider the line $(\overline{\boldsymbol{\Sigma}}, \boldsymbol{\Sigma}^{\mathrm{Trial}})$ and the intersection $\boldsymbol{\Sigma}^0$ between this line and the flow surface, boundary of $P^{\hom}$. $\boldsymbol{\Sigma}^0$ is unknown but the triaxiality ratio $\boldsymbol{\Sigma} - \overline{\boldsymbol{\Sigma}}$ is constant along the whole line $(\overline{\boldsymbol{\Sigma}}, \boldsymbol{\Sigma}^{\mathrm{Trial}})$. In particular

$$\frac{\Sigma_m^0 - \overline{\Sigma}_m}{\Sigma_{\mathrm{eq}}^0} = \frac{\Sigma_m^{\mathrm{Trial}} - \overline{\Sigma}_m}{\Sigma_{\mathrm{eq}}^{\mathrm{Trial}}}. \tag{15}$$

On the other hand, the constitutive relation (9) gives

$$\Sigma_m^0 = \mathfrak{f}_m(\boldsymbol{D}), \quad \Sigma_{\mathrm{eq}}^0 = \mathfrak{f}_{\mathrm{eq}}(\boldsymbol{D}),$$

where $\boldsymbol{D}$ is the (unknown) outer normal vector to $P^{\hom}$ at $\boldsymbol{\Sigma}^0$. It should be noted that, by isotropy, $\mathfrak{f}$ depends only on the three invariants of $\boldsymbol{D}$ and since the constituents in the linear comparison composite used in the N-phase model are isotropic, $\mathfrak{f}$ depends only on the two first invariants D_m and D_{eq} of $\boldsymbol{D}$: $\mathfrak{f}(D_m, D_{\mathrm{eq}})$. Furthermore, being a positively homogeneous function of

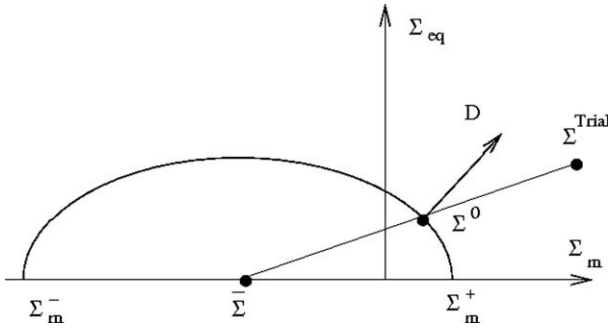

Fig. 1. Determination of interior points of $P^{\hom}$.

degree 0 with respect to $\boldsymbol{D}$, $\mathfrak{f}$ depends only on its triaxiality ratio $\theta = D_m/D_{\text{eq}} : \mathfrak{f}(D_m, D_{\text{eq}}) = \mathfrak{f}(\theta, 1)$. According to (15), θ solves the nonlinear equation

$$\frac{\mathfrak{f}_m(\theta,1) - \overline{\Sigma}_m}{\mathfrak{f}_{\text{eq}}(\theta,1)} = \frac{\Sigma_m^{\text{Trial}} - \overline{\Sigma}_m}{\Sigma_{\text{eq}}^{\text{Trial}}}, \tag{16}$$

which can be solved for θ using a Newton–Raphson algorithm. Then the two first invariants of $\boldsymbol{\Sigma}^0$ are given by

$$\Sigma_m^0 = \mathfrak{f}_m(\theta,1), \quad \Sigma_{\text{eq}}^0 = \mathfrak{f}_{\text{eq}}(\theta,1).$$

Finally, $\boldsymbol{\Sigma}^{\text{Trial}}$ is in P^{hom} if its invariants belong to the segment $[\overline{\boldsymbol{\Sigma}}, \boldsymbol{\Sigma}^0]$.

4. Applications

The above model has been implemented numerically to study the influence of the different parameters on the void growth in specific situations. The material data (Young modulus E, Poisson ratio ν and yield stress σ_0) of compact (unvoided) UO_2 at 1700 °C are

$$E = 173 \text{ GPa}, \quad \nu = 0.33, \quad \sigma_0 = 55 \text{ MPa}.$$

The original Gurson criterion ($q_1 = q_3 = 1$) is used to describe the plastic properties at the mesoscopic level (porous grains).

The applied loading is a purely hydrostatic deformation

$$\boldsymbol{E}(t) = E_m(t)\boldsymbol{i},$$

superimposed to internal pressures p_e and p_b which are kept constant in time along the loading path. More general loading paths including change in internal pressures could be explored using the algorithm described in Section 3 but, for simplicity, this direction is not pursued here. The overall stress is hydrostatic and the stress–strain response is represented by (Σ_m, E_m) plots.

4.1. Influence of the initial microstructure

The influence of the initial microstructure on the overall stress–strain curve is examined by varying the initial conditions f_b^0, f_e^0, w^0. The relative importance of the initial intragranular porosity f_b^0 and of the initial intergranular porosity f_e^0 is shown in Fig. 2a and b, respectively. For this particular choice of the aspect ratio $w = 0.1$ which corresponds to flat ellipsoids, the overall response is more sensitive to variations in f_e. However, the volume fraction f_e varies linearly with the aspect ratio w and therefore, for fixed f_e, smaller w corresponds to a higher density of voids, and therefore to a more severe damage. The influence of f_e is less pronounced when the intergranular voids tend to be spherical.

The influence of the initial aspect ratio w^0 is illustrated in Fig. 3. The initial porosity f_e^0 is the same in all plots while the aspect ratio w^0 is varied from 0.9 to 0.1. The density of voids increases while the aspect ratio decreases, resulting again in a more severe damage of the material when w is small.

4.2. Influence of the two internal pressures

The effect of the internal pressures p_e and p_b is discussed in Fig. 4. Note that the initial overall stress Σ_m is negative (when $E_m = 0$). Indeed, the internal pressure in the voids creates a dilatational eigenstrain in the matrix which is inhibited by the

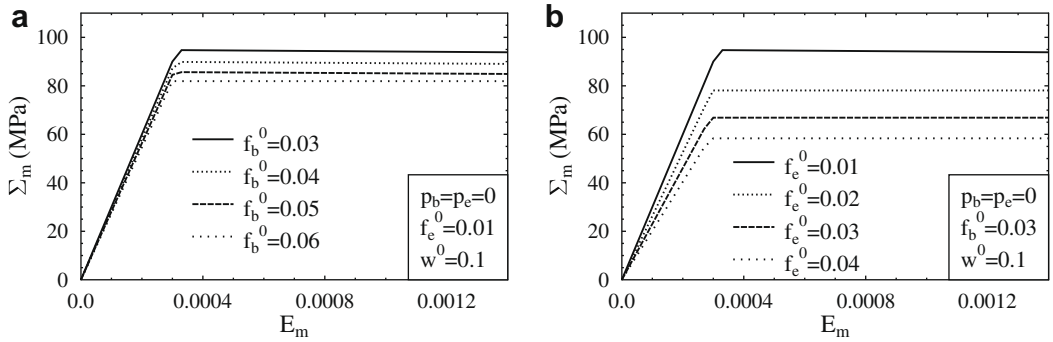

Fig. 2. Influence of the initial porosities f_e^0 and f_b^0 on the overall stress–strain response of a doubly voided material. Initial aspect ratio of the ellipsoidal cavities $w^0 = 0.1$. Drained case $p_e = p_b = 0$. (a) Influence of the intragranular porosity f_b^0 (spherical voids). (b) Influence of the intergranular porosity f_e^0 (ellipsoidal voids).

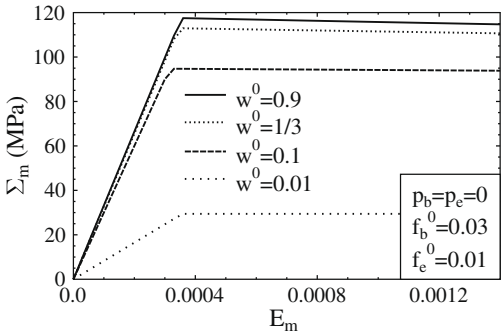

Fig. 3. Influence of the initial aspect ratio w^0 of the intergranular voids. Drained case $p_e = p_b = 0$.

condition $E_m = 0$ and a negative overall stress is required to enforce this constraint. For moderate values of p_e and p_b, the matrix does not yield under purely internal pressure in the two populations of voids and the resulting overall stress is purely elastic. It can be estimated by the relation (8) where the strain (which, again, is purely elastic) is 0, as $\Sigma_m = -b_2(p_e - b_1 p_b) - b_1 p_b$. It is also observed that the relative influence of p_e and p_b depends strongly on the aspect ratio w of the ellipsoidal voids. When the ellipsoidal voids are almost spherical in shape ($w = 0.9$, Fig. 4a and b) the influence of p_b is stronger than that of p_e (in this example where $f_b > f_e$). By contrast, when the voids are flat ($w = 0.1$, Fig. 4c and d) the influence of p_e is dominant. So, the relative influence of the two internal pressures is itself strongly influenced by the shape of the ellipsoidal intergranular voids. The loading is strain-controlled which allows for capturing a softening in the stress–strain curve.

All curves show a more or less steady softening of the material and no instability (in the sense of a sudden drop in the stress–strain curve) was observed in all the examples which have been considered here (which correspond to realistic values of the porosities). Additional ingredients are required in order to observe instabilities related to the coalescence of voids. This is the object of the next section.

4.3. Influence of the presence of intragranular voids on the growth of the intergranular voids

In a recent study on voided materials with two populations of spherical voids, Fabrègue and Pardoen, (2008) have observed that at low stress triaxiality the presence of small voids has no significant influence on the growth of larger voids.

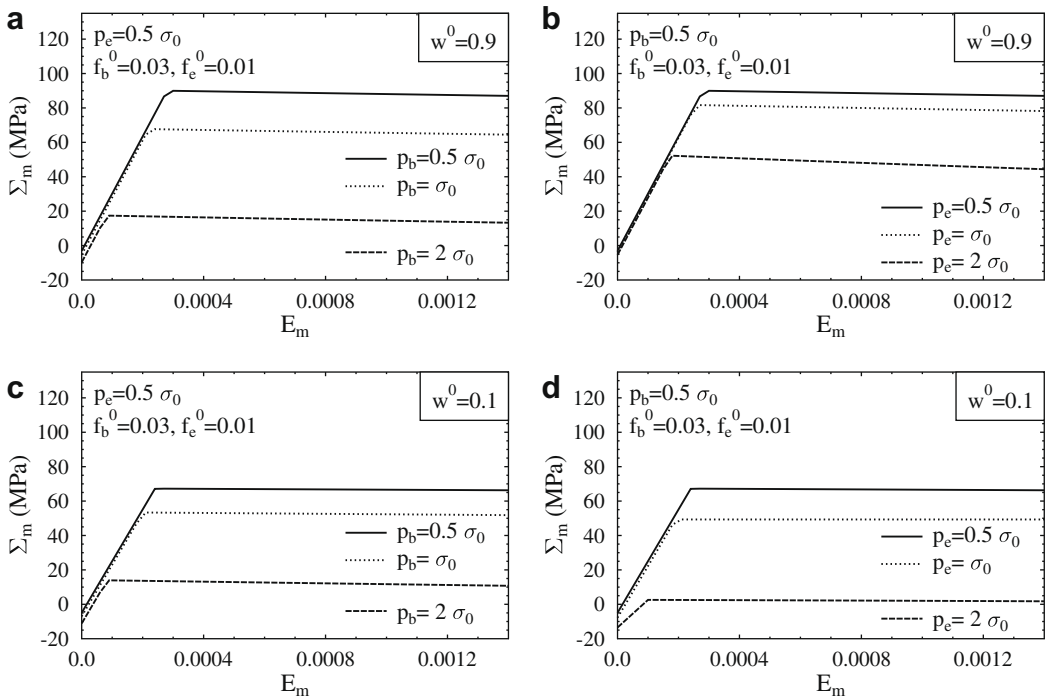

Fig. 4. Influence of the internal pressures p_b and p_e on the overall stress–strain response of a doubly voided material. Initial aspect ratio of the ellipsoidal cavities $w^0 = 0.9, 0.2, 0.1$.

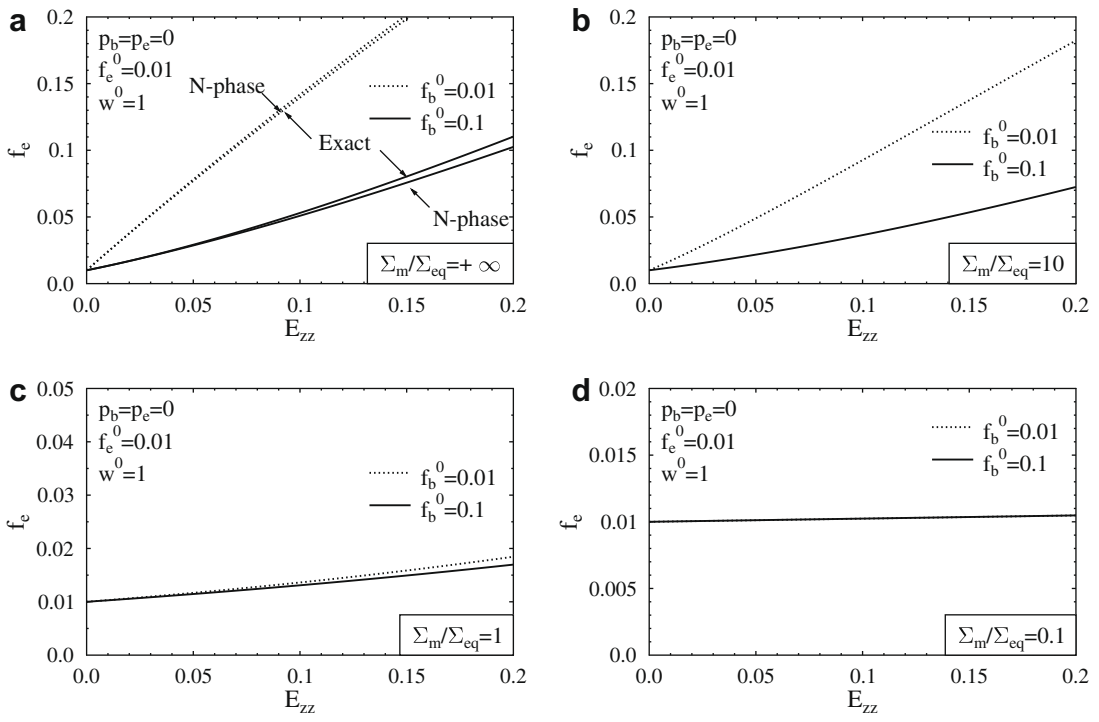

Fig. 5. Influence of the presence of a secondary population of voids (small voids) on the growth of the first population (large voids). Influence of the overall stress triaxiality $T = \Sigma_m/\Sigma_{eq}$. Drained material $p_b = p_e = 0$. All predictions, except the exact result, are obtained with the N-phase model with $N = 11$.

The present model shows similar trends at low stress triaxialities. However, it does show a significant influence of the population of small voids on the growth of the larger voids at high stress triaxiality.

Consider first a hollow sphere made of a Gurson matrix (porosity f_b) with a central cavity (volume fraction f_e). A hydrostatic deformation $E_m(t)$ is applied to this hollow sphere and the void volume fractions $f_b(r, E_m)$ and $f_e(E_m)$ can be computed, either analytically, or in our case, using the N-phase secant method (which delivers the exact response in the limit of a large number of layers N). Note that, in the exact solution, the secondary porosity f_b has a gradient in the radial direction. The prediction of the N-phase model for the evolution of f_e are compared to the exact solution in Fig. 5a for different initial volume fraction of the small voids. According to assumption (H1), the model does not account for the heterogeneity of the distribution of f_b in the matrix and makes the approximation that the spatially inhomogeneous field f_b can be replaced by a single scalar value which acts as an effective porosity. This explains the difference between the exact solution and the predictions of the model, which however is small as can be seen in Fig. 5a. A second observation, valid both for the exact solution and for the model, is that the small voids delay the growth of the large voids. This is due to the fact that the test is driven by the overall strain and part of this overall strain contributes to the growth of the smaller voids. Therefore, the dilatation of the large voids is smaller when the volume fraction of the small voids is larger.

Considering that the comparison between the exact solution and the model is satisfactory, other stress triaxiality ratios have been considered. No analytical solution is available, and therefore only the predictions of the present model are shown. The material containing two populations of voids is deformed axisymmetrically (the axis of symmetry being the z direction) along a path where the stress triaxiality is prescribed $\Sigma_m/\Sigma_{eq} = 10, 1, 0.1$ and two different values of the secondary porosity f_b^0. The evolution of the porosity f_e predicted by the model is shown in Fig. 5b–d. The observation of Fabrègue and Pardoen (2008) made on the basis of finite element simulations is retrieved by the model at low stress triaxiality ($\Sigma_m/\Sigma_{eq} = 0.1, 1$). But significant deviations from this result are observed at large stress triaxiality ($\Sigma_m/\Sigma_{eq} = 10, +\infty$).

5. Void coalescence

5.1. Onset of coalescence

The ultimate stage of void growth is the coalescence of several voids which eventually results in the formation of a macroscopic crack. In the present problem, the macro-cracks formed by void coalescence can link together and give rise to a connected network of cracks through which fission gases may diffuse and reach the outer barrier. Predicting void coalescence is therefore an important safety issue. The evolution equations derived in Section 2.2 are based on certain geometrical

assumptions, such as well-separated and self-similar ellipsoids, which are inappropriate at the onset of coalescence. These evolution equations capture correctly the evolution of the voids when all voids deform in a similar manner in a diffuse plasticity mode. But at a certain point, a few voids start growing much more rapidly than others and an unstable process takes place. This change of regime is now well-recognized. It was first modelled by Koplik and Needleman, 1988 by the introduction in the GTN criterion of an effective porosity f^* growing more rapidly than the actual porosity. This model requires the fit of several parameters which can be questioned. Another interpretation of coalescence, which will be followed in this study, is that the transition to coalescence corresponds to the localization of the plastic deformation in the ligament between two neighbouring voids.

For materials containing a single population of voids, Thomason, 1985 has derived an empirical expression based on slip-line fields between voids arranged periodically in a rigid ideally plastic matrix. For a spherical cavity with radius b_1 in a cylindrical block of matrix with radius b_2 and axis aligned in the z direction, subjected to an axisymmetric stress state with $\Sigma_{zz} \geqslant \Sigma_{xx} = \Sigma_{yy}$, Thomason's criterion reads as $\Sigma_{zz} \leqslant \Sigma_{zz}^{\mathrm{Tho}}$ with (Benzerga, 2002)

$$\Sigma_{zz}^{\mathrm{Tho}} = \sigma_0(1-\chi_{\mathrm{Tho}}^2)C_{\mathrm{Tho}} \qquad \text{where} \quad \chi_{\mathrm{Tho}} = \frac{b_1}{b_2}, \quad C_{\mathrm{Tho}} = 0.1\left(\frac{1}{\chi_{\mathrm{Tho}}}-1\right)^2 + 1.2\sqrt{\frac{1}{\chi_{\mathrm{Tho}}}}. \tag{17}$$

Thomason's criterion has been generalized to ellipsoidal voids with ellipsoidal distribution by Pardoen and Hutchinson, 2000 and Benzerga, 2002:

$$\Sigma_{zz} \leqslant \Sigma_{zz}^{Ben}, \quad \Sigma_{zz}^{Ben} = \sigma_0(1-\chi_{\mathrm{Ben}}^2)C_{\mathrm{Ben}}, \qquad \text{where} \quad \chi_{\mathrm{Ben}} = \frac{b_1}{b_2},$$
$$C_{\mathrm{Ben}} = 0.1\left(\frac{\chi_{\mathrm{Ben}}^{-1}-1}{w^2+0.1\chi_{\mathrm{Ben}}^{-1}+0.02\chi_{\mathrm{Ben}}^{-2}}\right)^2 + 1.3\sqrt{\frac{1}{\chi_{\mathrm{Ben}}}}. \tag{18}$$

It will be convenient to use the triaxial form of this criterion (Benzerga, 2002; Pardoen and Hutchinson, 2003)

$$\Sigma_{\mathrm{eq}} + \frac{3}{2}\,|\,\Sigma_h\,| - \frac{3}{2}\sigma_0(1-\chi_{\mathrm{Ben}}^2)C_{\mathrm{Ben}} \leqslant 0, \tag{19}$$

where $\Sigma_h = 2\alpha_2\Sigma_p + (1-2\alpha_2)\Sigma_n$ is the generalized "hydrostatic" stress of Gologanu et al., 1994. Σ_n is the stress in the direction of the axis of symmetry of the ellipsoid, while Σ_p is the axisymmetric stress in the plane perpendicular to this axis and α_2 is a geometrical parameter whose definition is recalled in Appendix A.

The aim of the following section is to show how the criteria (17) or (18), derived for a single population of voids, can be used in the present context of doubly voided materials.

5.2. Composite grain model

In order to use the coalescence criteria, more specific information about the microstructure of the doubly voided material has to be introduced. So far, the only information on the microstructure which has been used is the fact that spheroidal voids are randomly distributed in a Gurson matrix. In the problem of fragmentation of a UO_2 under the action of high-pressure fission gases contained in the two population of voids, the typical situation, shown in Fig. 6 right, is a grain weakened by spherical voids in its interior and surrounded by a grain boundary zone where ellipsoidal voids parallel to the grain boundary are located. This situation can be schematized by considering a single grain as a composite sphere Ω as represented in Fig. 6. The inner core $\Omega^{(1)}$ contains small spherical voids with porosity f_b, subjected to an internal pressure p_b. The outer spherical

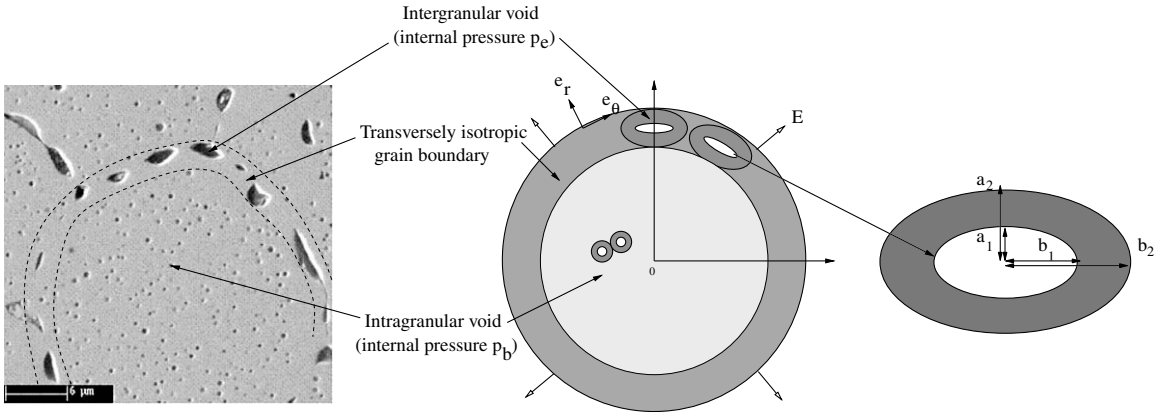

Fig. 6. Actual and idealized geometry of a grain. Composite Grain Model.

shell represents an interphase layer around the grain boundary between two adjacent grains. This layer contains spheroidal voids with minor axis aligned in the radial direction. These intergranular voids with volume fraction f_e are subjected to an internal pressure p_e. The whole model will be referred to as the *Composite Grain Model*.

R_1 and R_2 denote the radii of $\Omega^{(1)}$ and Ω, respectively. The interphase zone around the grain boundary is denoted by $\Omega^{(2)} = \Omega - \Omega^{(1)}$. $f^{(1)}$ and $f^{(2)}$ denote the volume fraction of $\Omega^{(1)}$ and $\Omega^{(2)}$ relative to the whole volume element Ω. The thickness of the grain boundary interphase $2a_2 = R_1 - R_2$ is unknown at this stage and will be specified in due course.

The inner core contains only spherical voids and its behaviour can be modelled using the plastic dissipation potential φ^{Gur} of Gurson, 1977. The outer shell contains ellipsoidal voids with a definite orientation and its behaviour can therefore be modelled using the effective potential φ^{Gol} of Gologanu et al., 1994 which describes the effective relations of a von Mises matrix containing aligned ellipsoidal voids. The boundary zone contains a single void through its thickness and the use of an effective potential can be questioned. In fact the derivation of the potential of Gologanu et al., 1994 was carried out on a single void and does not assume the presence of many voids. Its use is therefore legitimate in the present context. For simplicity, elasticity is neglected in both phases and the total strain-rate can be identified with the plastic strain-rate.

The loading conditions depend on three independent parameters, the two internal pressures p_b and p_e and the hydrostatic deformation applied on the external boundary of the volume through an imposed velocity $\dot{\boldsymbol{u}} = \dot{E}_m \boldsymbol{i} \cdot \boldsymbol{x}$ on $\partial\Omega$. The problem to be solved on Ω reads as

$$\begin{aligned} &\boldsymbol{\sigma} + p_b \boldsymbol{i} = \frac{\partial \varphi^{\mathrm{Gur}}}{\partial \dot{\boldsymbol{\varepsilon}}}(\dot{\boldsymbol{\varepsilon}}) \quad \text{in } \Omega^{(1)}, \qquad \boldsymbol{\sigma} + p_e \boldsymbol{i} = \frac{\partial \varphi^{\mathrm{Gol}}}{\partial \dot{\boldsymbol{\varepsilon}}}(\dot{\boldsymbol{\varepsilon}}) \quad \text{in } \Omega^{(2)} \\ &\mathrm{div}(\boldsymbol{\sigma}) = \boldsymbol{0} \quad \text{in } \Omega, \qquad \dot{\boldsymbol{u}} = \dot{\boldsymbol{E}} \cdot \boldsymbol{x} \quad \text{on } \partial\Omega. \end{aligned} \tag{20}$$

Detailed expressions for the potentials φ^{Gur} and φ^{Gol} will be given in due course. As in the first part of this study, one of the two internal pressures can be eliminated by shifting the stress field. Here it is chosen to eliminate the pressure in the ellipsoidal voids by setting $\boldsymbol{\sigma}_e = \boldsymbol{\sigma} + p_e \boldsymbol{i}$. The local problem (20) is equivalent to

$$\begin{aligned} &\boldsymbol{\sigma}_e + p\boldsymbol{i} = \frac{\partial \varphi^{\mathrm{Gur}}}{\partial \dot{\boldsymbol{\varepsilon}}}(\dot{\boldsymbol{\varepsilon}}) \quad \text{in } \Omega^{(1)}, \qquad \boldsymbol{\sigma}_e = \frac{\partial \varphi^{\mathrm{Gol}}}{\partial \dot{\boldsymbol{\varepsilon}}}(\dot{\boldsymbol{\varepsilon}}) \quad \text{in } \Omega^{(2)}, \\ &\mathrm{div}(\boldsymbol{\sigma}_e) = \boldsymbol{0} \quad \text{in } \Omega, \qquad \dot{\boldsymbol{u}} = \dot{\boldsymbol{E}} \cdot \boldsymbol{x} \quad \text{on } \partial\Omega, \end{aligned} \tag{21}$$

where $p = p_b - p_e$. The macroscopic stress is then obtained as

$$\boldsymbol{\Sigma} = \langle \boldsymbol{\sigma} \rangle_\Omega = \frac{1}{|\Omega|} \int_\Omega \boldsymbol{\sigma} d\Omega = \langle \boldsymbol{\sigma}_e \rangle_\Omega - p_e \boldsymbol{i}. \tag{22}$$

For simplicity, the local fields $(\boldsymbol{\sigma}_e, \dot{\boldsymbol{\varepsilon}})$ solution of (21) will be denoted as $(\boldsymbol{\sigma}, \dot{\boldsymbol{\varepsilon}})$ in the sequel.

5.3. Approximate resolution of the local problem (21)

5.3.1. Formulation of the nonlinear problem with secant moduli

The exact resolution of the nonlinear problem (21) is difficult (and its solution is not known to the best of the authors' knowledge). An approximate resolution by the modified secant method (which is another name for the variational procedure of Ponte Castañeda, 1991) is adopted. The error due to the substitution of a nonlinear medium by an optimal linear composite is expected to be small for the following reasons. First, due to the spherical symmetry of the loading and of the geometry, the core of the grain is subjected to an hydrostatic stress on its outer boundary $r = R_1$. Therefore the stress field, as well as the strain-rate field, inside the core is uniform and hydrostatic. There is no error induced by the modified secant method for uniform stress fields. Second the outer shell is thin and the stress, or strain-rate, heterogeneity in the grain boundary region is limited.

The application of the modified secant method requires some care. The axes of symmetry of the material in the outer layer corresponding to the grain boundary are in the radial direction and therefore differ for points having different Euler angles. As a consequence, the composite grain model is, in full rigor, a composite with an infinite number of different phases (different orientations in the outer layer) and not a two-phase composite. However, when the composite grain is subjected to an outer isotropic deformation and internal pressure in the voids, the solution of the nonlinear problem has the same spherical symmetry as the data and the strain-rate field is hydrostatic in the central core and has only two independent components $\dot{\varepsilon}_{rr}(r)$ and $\dot{\varepsilon}_{\theta\theta}(r) = \dot{\varepsilon}_{\phi\phi}(r)$ in the outer layer. The linear comparison composite is consequently chosen with the same spherical symmetry, isotropic in the core, and locally transversally isotropic in the outer shell. By "locally" it is meant that the invariant direction is the direction $\boldsymbol{e}_r$ which depends on the Euler angles of the point under consideration. The linear comparison composite is not a two-phase composite for the same reason as for the nonlinear composite, but is characterized by four elastic coefficients, a bulk modulus in the core and three elastic coefficients in the outer layer.

In order to derive analytical expressions for these elastic coefficients, note that, the strain-rate and the stress field are isotropic in the core and are related by

$$\sigma_m + p = \frac{1}{3} \frac{\partial \varphi^{\mathrm{Gur}}}{\partial \dot{\varepsilon}_m}(\dot{\varepsilon}_m \boldsymbol{i}) = 3k_{\mathrm{sct}} \dot{\varepsilon}_m,$$

where

$$\varphi^{\mathrm{Gur}}(\dot{\boldsymbol{\varepsilon}}) = \sigma_0 \int_{f_b}^{1} \sqrt{\frac{4\dot{\varepsilon}_m^2}{t^2} + \dot{\varepsilon}_{\mathrm{eq}}^2}\,\mathrm{d}t, \qquad k_{\mathrm{sct}} = -\frac{2}{9}\sigma_0 \frac{1}{\sqrt{\dot{\varepsilon}_m^2}} \ln(f_b). \tag{23}$$

In the outer layer, the potential $\varphi^{\mathrm{Gol}}(\dot{\boldsymbol{\varepsilon}})$ can be expressed as

$$\varphi^{\mathrm{Gol}}(\dot{\boldsymbol{\varepsilon}}) = \sigma_0' \int_{\hat{f}}^{1} \sqrt{\frac{\tilde{y}_2^2}{t^2}(\overline{F}\mathscr{A} + \overline{G}\mathscr{B})^2 + \overline{H}^2\mathscr{B}^2}\,\mathrm{d}t, \tag{24}$$

where $\mathscr{A}$ and $\mathscr{B}$ are functions of $\dot{\boldsymbol{\varepsilon}}$ and where $y_2, \overline{F}, \overline{G}, \overline{H}, \sigma_0'$ are geometrical or material constants (see Appendix A for detailed expressions). After use of the equality $\dot{\varepsilon}_{\theta\theta} = \dot{\varepsilon}_{\phi\phi}$, one obtains the secant relations

$$\sigma_{rr} = n_{\mathrm{sct}}\dot{\varepsilon}_{rr} + 2l_{\mathrm{sct}}\dot{\varepsilon}_{\theta\theta}, \qquad \sigma_{\theta\theta} = l_{\mathrm{sct}}\dot{\varepsilon}_{rr} + 2\kappa_{\mathrm{sct}}\dot{\varepsilon}_{\theta\theta}, \tag{25}$$

where the secant moduli n_{sct}, l_{sct} and κ_{sct} are given by (A.4), (A.5) and (A.6). They depend, at each point $\boldsymbol{x}$, on the strain-rate $\dot{\boldsymbol{\varepsilon}}(\boldsymbol{x})$ at this point. The idea underlying the variational or secant method (and all methods making use of a linear comparison composite) is to replace these nonuniform moduli by uniform moduli per phase.

5.3.2. Linear comparison composite (LCC)

Now consider a linear composite with a central core with bulk modulus $k^{(1)}$ and a locally transversely isotropic outer layer characterized by elastic moduli $(n^{(2)}, l^{(2)}, \kappa^{(2)})$. The local elastic energy of the linear comparison composite in the core and in the outer layer can be, respectively, written as

$$w_0^{(1)}(\dot{\boldsymbol{\varepsilon}}) = \frac{9k^{(1)}}{2}\dot{\varepsilon}_m^2 - 3p\dot{\varepsilon}_m, \qquad w_0^{(2)}(\dot{\boldsymbol{\varepsilon}}) = \frac{1}{2}(n^{(2)}\dot{\varepsilon}_{rr}^2 + 4l^{(2)}\dot{\varepsilon}_{rr}\dot{\varepsilon}_{\theta\theta} + 4\kappa^{(2)}\dot{\varepsilon}_{\theta\theta}^2).$$

Consequently, for the hydrostatic loading conditions under consideration here, the effective energy of the linear comparison composite can be expressed as

$$w_0^{\mathrm{hom}}(\dot{E}_m, p) = f^{(1)}\left(\frac{9}{2}k_0\langle\dot{\varepsilon}_m^2\rangle_1 - 3p\langle\dot{\varepsilon}_m\rangle_1\right) + f^{(2)}\left(\frac{n^{(2)}}{2}\langle\dot{\varepsilon}_{rr}^2\rangle_2 + 2l^{(2)}\langle\dot{\varepsilon}_{rr}\dot{\varepsilon}_{\theta\theta}\rangle_2 + 2\kappa^{(2)}\langle\dot{\varepsilon}_{\theta\theta}^2\rangle_2\right),$$

from which it follows that the second moments of the strain field in the phases of the LCC are given as

$$\begin{aligned} \langle\dot{\varepsilon}_m^2\rangle_1 &= \frac{2}{9f^{(1)}}\frac{\partial w_0^{\mathrm{hom}}}{\partial k^{(1)}}(\dot{E}_m, p), \qquad \langle\dot{\varepsilon}_{rr}^2\rangle_2 = \frac{2}{f^{(2)}}\frac{\partial w_0^{\mathrm{hom}}}{\partial n^{(2)}}, \\ \langle\dot{\varepsilon}_{rr}\dot{\varepsilon}_{\theta\theta}\rangle_2 &= \frac{1}{2f^{(2)}}\frac{\partial w_0^{\mathrm{hom}}}{\partial l^{(2)}}, \qquad \langle\dot{\varepsilon}_{\theta\theta}^2\rangle_2 = \frac{1}{2f^{(2)}}\frac{\partial w_0^{\mathrm{hom}}}{\partial \kappa^{(2)}}. \end{aligned} \tag{26}$$

The modified secant method consists in choosing the elastic moduli $k^{(1)}, n^{(2)}, l^{(2)}, \kappa^{(2)}$ in the linear comparison composite using the second-moment of the strain field over each individual phase, using the relations (23), (A.4), (A.5), (A.6) and (26).

5.3.3. Implementation

The modified secant method for the specific problem under consideration can be summarized as

Input: $\dot{E}_m$.
Do until convergence:
(1) *Compute the secant moduli*

$k^{(1)} = k_{\mathrm{sct}}(\langle\dot{\varepsilon}_m^2\rangle_1)$ *by relation* (23),

$n^{(2)}, l^{(2)}, \kappa^{(2)} = n_{\mathrm{sct}}, l_{\mathrm{sct}}, \kappa_{\mathrm{sct}}(\langle\dot{\varepsilon}_{rr}^2\rangle_2, \langle\dot{\varepsilon}_{\theta\theta}^2\rangle_2, \langle\dot{\varepsilon}_{rr}\dot{\varepsilon}_{\theta\theta}\rangle_2)$ *by relations (A.4)–(A.6),*

(2) *Compute the second moments* $\langle\dot{\varepsilon}_{rr}^2\rangle_2, \langle\dot{\varepsilon}_{rr}\dot{\varepsilon}_{\theta\theta}\rangle_2, \langle\dot{\varepsilon}_{\theta\theta}^2\rangle_2$ *by relations (26) where the effective energy* $w_0^{\mathrm{hom}}(\dot{E}_m, p)$ *is given by relation (B.9).*

Output:

$$\Sigma_m + p_e = 3k^{\mathrm{hom}}\dot{E}_m - pb^{\mathrm{hom}},$$

where k^{hom} and b^{hom} are given by the relations (B.24) and (B.25), respectively, $p = p_b - p_e$ and $\boldsymbol{\Sigma}$ is the actual stress (22) in the composite grain.

5.4. Microstructure evolution

When the loading is applied to the composite grain under the form of a path $E_m(t), p_e(t), p_b(t)$, its microstructure evolves. The spherical symmetry of the problem allows us to assume that the spherical voids in the core remain spherical and that the spheroidal voids in the outer layer remain spheroidal. Five microstructural variables

$$f_b, f_e^*, w, R_1, R_2$$

are sufficient to specify completely the microstructure, where f_e^* is the relative porosity of the intergranular voids in the outer layer related to the absolute intergranular porosity f_e by $f_e = f_e^* f^{(2)}$.

The other microstructural parameters $a_1, a_2, b_1, b_2, f^{(1)}$ are related to these five variables through the relations

$$b_2^2 - a_2^2 = b_1^2 - a_1^2 \text{ (confocality)}, \quad w = \frac{a_1}{b_1}, \quad \frac{a_1 b_1^2}{a_2 b_2^2} = f_e^*, \quad 2a_2 = R_2 - R_1, \quad f^{(1)} = \frac{R_1^3}{R_2^3}. \tag{27}$$

The mass balance equations in phase 1 and 2 give the two evolution equations (28), elementary geometrical considerations give the two other evolution equations (29) and the last equation governing the change in the aspect ratio w is taken from Gologanu et al., 1994

$$\dot{f}_b = 3(1-f_b)\langle \dot{\varepsilon}_m \rangle_1, \quad \dot{f}_e^* = 3(1-f_e^*)\langle \dot{\varepsilon}_m \rangle_2, \tag{28}$$

$$\dot{R}_1 = R_1 \langle \dot{\varepsilon}_m \rangle_1, \quad \dot{R}_2 = R_2 \dot{E}_m, \tag{29}$$

$$\dot{w} = w\left(\langle \dot{\varepsilon}_{rr} - \dot{\varepsilon}_{\theta\theta} \rangle_2 + 3\left(\frac{1-3\alpha_1}{f_e^*} + 3\alpha_2 - 1 \right) \langle \dot{\varepsilon}_m \rangle_2 \right), \tag{30}$$

where α_1 and α_2 are geometrical parameters defined in Appendix A. The first moments of the strain-rate field in the phases are estimated as the first moments of the strain field in the LCC and are given in Appendix B, Eq. (B.29).

5.5. Void coalescence

The evolution equations (28)–(30) are integrated in time along a loading path $E_m(t), p(t)$. The average stresses in each phase are estimated in the LCC and in particular

$$\langle \sigma_m \rangle_1 = 3k^{(1)} \langle \dot{\varepsilon}_m \rangle_1 - p, \quad \langle \sigma_{rr} \rangle_2 = n^{(2)} \langle \dot{\varepsilon}_{rr} \rangle_2 + 2l^{(2)} \langle \dot{\varepsilon}_{\theta\theta} \rangle_2, \quad \langle \sigma_{\theta\theta} \rangle_2 = l^{(2)} \langle \dot{\varepsilon}_{rr} \rangle_2 + 2\kappa^{(2)} \langle \dot{\varepsilon}_{\theta\theta} \rangle_2, \tag{31}$$

where $k^{(1)}$, $n^{(2)}$, $l^{(2)}$ and $\kappa^{(2)}$ are the elastic coefficients given at convergence by the modified secant method. The composite grain is deformed until coalescence is detected in either phase (core or outer layer) by one of the criteria (17) or (18).

In the core, coalescence is detected by the Thomason's criterion (17) applied to the average stress in the core (the stress is indeed uniform and hydrostatic in the core). In its original form the criterion of Thomason, 1985 applies to stress-free voids in an incompressible von Mises material. Thanks to the matrix incompressibility, the application of an internal pressure p in the spherical voids results in a shift of the original criterion which now reads as

$$| \langle \sigma_m \rangle_1 + p | \leqslant \Sigma^{\text{Tho}}. \tag{32}$$

In the outer layer, coalescence is detected by the criterion (19)

$$| \langle \sigma_{rr} - \sigma_{\theta\theta} \rangle_2 | + \frac{3}{2} | 2\alpha_2 \langle \sigma_{\theta\theta} \rangle_2 + (1-2\alpha_2) \langle \sigma_{rr} \rangle_2 | - \frac{3}{2} \sigma_0 (1 - \chi_{\text{Ben}}^2) C_{\text{Ben}} \leqslant 0. \tag{33}$$

Failure of the whole grain is assumed to take place as soon as one of the two criteria (32) or (33) is attained. Failure is said to be *transgranular* when (32) is attained first and *intergranular* when (33) is attained first.

5.6. Discussion

The above composite grain model consisting of the evolution equations (28)–(30), together with the secant approximation is used to predict the type of failure and the strain at failure of polycrystalline voided materials with intragranular and intergranular voids. For this purpose, one has to determine the initial aspect ratio w^0 of the voids and the initial width of the grain boundary zone $2a_2^0$ which was left undetermined by the above analysis. The aspect ratio can be estimated from the micrograph shown in Fig. 6 to be $w^0 \simeq 1/3$. Similarly the initial width of the grain boundary can be roughly estimated from Fig. 6 as about one fifth of the grain radius, leading to an initial width $a_2^0/R_2^0 = 0.1$, where R_2^0 is the average grain size. It can also be estimated by matching the prediction of the composite grain model with that of the N-phase model in the range where the two models can be compared, i.e. in the range of incipient plastic deformation where plasticity is still diffuse. The predictions of both models are shown in Fig. 7 with $a_2^0/R_2^0 = 0.1$ with due account for changes in microstructure. As can be seen, the maximal stresses are very close to each other and the models differ only slightly in the softening regime.

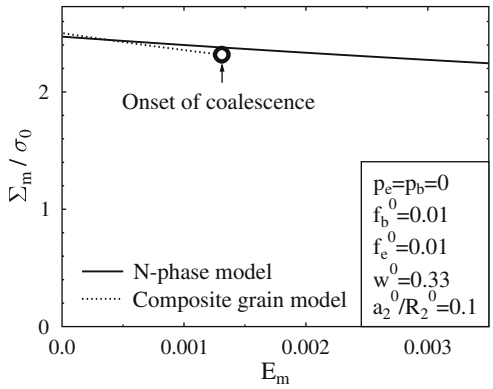

Fig. 7. Onset of void coalescence detected by the composite grain model.

The difference is that the composite grain model is able to predict void coalescence in the phases, whereas the *N*-phase model is not.

All results shown in the rest of this section are obtained with $a_2^0/R_2^0 = 0.1, w^0 = 1/3$.

A parametric study of the influence of the initial geometrical parameters f_e^0, f_b^0 and of the loading parameters p_e and p_b is carried out. The pressures p_e and p_b are prescribed and constant in time, whereas the dilatational strain E_m is increased linearly with time until coalescence is reached in one of the two regions in the composite grain. Transgranular failure is represented by a dark core surrounded by a white annulus, whereas intergranular failure is shown by a dark annulus and a white core (the phase undergoing failure is shown in dark).

Influence of internal pressures. The influence of the internal pressures p_e and p_b is shown in Fig. 8. The pressure p_b has a strong influence both on the maximum stress, on the type of failure and on the overall ductility of the composite grain. When p_b is zero or small, the failure occurs at the grain boundary at a relatively small overall strain. However when p_b is larger than

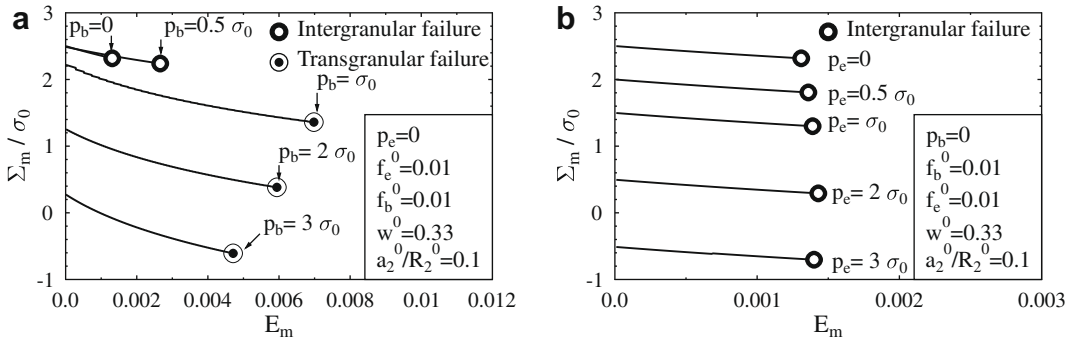

Fig. 8. Influence of the internal pressures p_b and p_e on the overall stress–strain response of a doubly voided material.

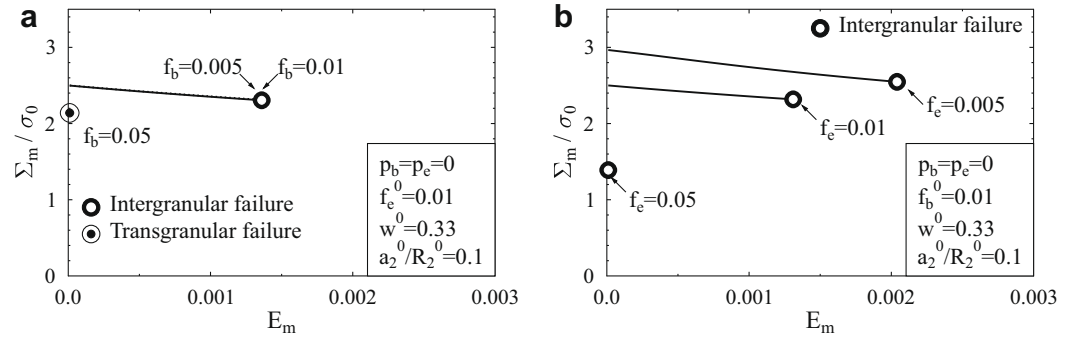

Fig. 9. Influence of the two porosities f_b and f_e on the overall stress–strain response of a doubly voided material.

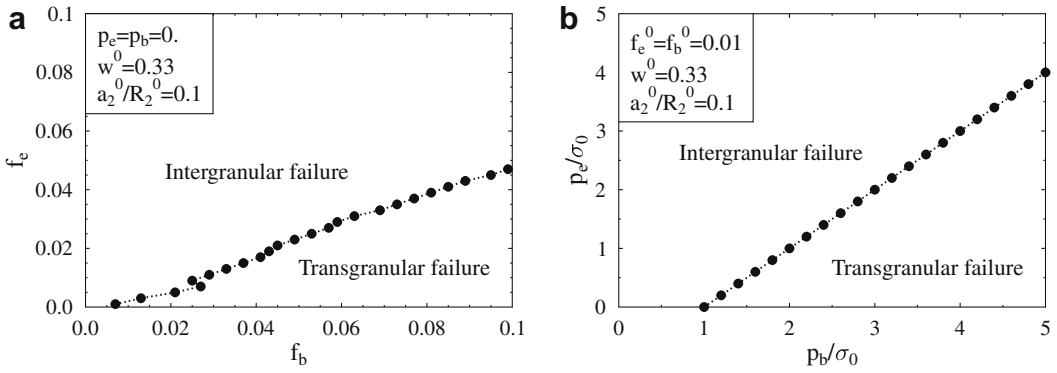

Fig. 10. Influence of the geometrical parameters w and b_2 on the overall stress–strain response of a doubly voided material.

σ_0 (this threshold depends on the other parameters) the failure becomes transgranular and the overall ductility increases. The pressure p_b creates an initial compression in the grain boundary region which delays the failure of this region.

By contrast, the internal pressure p_e in the intergranular voids promotes intergranular failure and has almost no influence on the overall ductility of the composite grain. It does have a significant influence on the maximal overall stress.

Influence of initial void volume fractions. The influence of the void volume fractions f_e and f_b is shown in Fig. 9. For small f_b (smaller than f_e in the present example) the failure is intergranular and f_b has little influence on the overall ductility. However when f_b is significantly larger than f_e the failure is transgranular and the overall ductility falls dramatically. The influence of f_b is seen to be more significant on the maximal strain than on the maximal stress.

The effect of the intergranular porosity shows similar trends. It can be seen in Fig. 10 that when f_e is significantly smaller than f_b the failure is transgranular whereas it becomes intergranular as soon as both porosities are of the same order (with the present set of the other parameters).

Transgranular versus intergranular failure. Finally it is possible to discuss the dependence of the type of failure on the initial void volume fractions and on the applied pressures. As shown in Fig. 10, intergranular failure is the predominant type of failure, but transgranular failure can also be observed. The line of separation between the regions corresponding to the two types of failure is almost straight, either in the (f_b, f_e) plane or in the (p_b, p_e) plane. For a drained material the effect of the intergranular void volume fraction is approximately twice that of the intragranular porosity (when $w = 1/3$). When the two volume fractions are small and of the same order, the separation between the two regimes is approximately ruled by the sign of $p_e - p_b - \sigma_0$. In particular a sufficiently high internal presssure p_b in the secondary voids is necessary to observe transgranular failure.

Merits and limits of the N-phase model and of the composite grain model. The *N*-phase model and the composite grain model have different ranges of validity and application. The *N*-phase model can be used for arbitrary triaxial loading conditions, whereas the composite grain model is limited to hydrostatic loadings. On the other hand, thanks to its specific geometry, the composite grain model is able to detect coalescence, either inside the grains or along the grain boundaries. The *N*-phase model does not incorporate enough specific microstructural information to be able to predict coalescence.

The two models are in fact complementary. When the polycrystalline microstructure is close to the one shown in Fig. 6 and when the loading consists of a pure dilatation and internal pressures, the composite grain model is the most appropriate one. However, when the ellipsoidal voids are dispersed in the porous matrix in a more random way, or if the applied strain (or stress) is not hydrostatic, the *N*-phase model is the most appropriate one. Predictions regarding the material ductility under more general loading conditions could be made by adopting a slightly different model for the grain boundary zone. The spherical model used here is adequate for hydrostatic strain (or stress). When the principal stresses are different, one could use a model similar to that of Pardoen et al. (2003) where the grain boundary is modelled as a thin layer bounded by two planes rather than by two spherical surfaces. The technical details would be different, but in spirit the model would be very similar.

6. Conclusion

In this study, we have developed a constitutive model for doubly voided materials which can predict the growth of the voids and, to a certain extent, their coalescence. This constitutive model consists, classically, of two parts:

- Instantaneous effective stress–strain relations were derived in part I of the study and the evolution equations derived in the present paper. Two rigorous upper bounds for the effective plastic potential were obtained. Each of these upper bounds has a different range of accuracy and none is accurate at all stress triaxiality. Therefore a *N*-phase model interpolating between these two upper bounds was proposed which improves on both bounds at all stress triaxialities.

- In the second part of this study (present paper), differential equations governing the evolution of the microstructural parameters in terms of the applied loading have been derived. The integration in time of these integration has been discussed and implemented. Void growth results in a global softening for the stress–strain response of the material. In particular this study has shown that the small voids have a significant effect on the growth of the larger voids at high triaxiality.
- In addition to these constitutive equations a simple model for the prediction of void coalescence has been proposed which can serve to predict the overall ductility of polycrystalline porous materials under the combined action of thermal dilatation and internal pressure in the voids.

Acknowledgement

This work was partly supported by the French Institut de Radioprotection et de Sûreté Nucléaire through the grant IRSN-CNRS 31002799. Fig. 6 (left) is adapted from Dubourg, Faure-Geors, Nicaise and Barrachin, Fission product release in the first two PHEBUS tests FPT0 and FPT1, Nuclear Engineering and Design 235, 2183–2208 (2005) with permission from Elsevier.

Appendix A. Secant moduli for the potential of Gologanu et al., 1994

Gologanu et al., 1994 have derived the following estimate for the effective dissipation potential of a porous material made of a von Mises matrix weakened by aligned spheroidal voids and subjected to an axisymmetric train-rate $\dot{\boldsymbol{\varepsilon}}$:

$$\varphi^{\mathrm{Gol}}(\dot{\boldsymbol{\varepsilon}}) = \sigma_0' \int_{\tilde{f}}^{1} \sqrt{\frac{\tilde{y}_2^2}{t^2}(\overline{F}\mathscr{A} + \overline{G}\mathscr{B})^2 + \overline{H}^2\mathscr{B}^2}\,\mathrm{d}t, \tag{A.1}$$

where $\mathscr{A}, \mathscr{B}$ are functions of the strain-rate $\dot{\boldsymbol{\varepsilon}}$, whereas the other coefficients are purely geometrical (or material) coefficients which do not depend on $\dot{\boldsymbol{\varepsilon}}$.

The purely geometrical parameters are

$$\begin{aligned}
&|\Omega| = \frac{4}{3}\pi a_2 b_2^2, \quad f = \frac{a_1 b_1^2}{a_2 b_2^2}, \quad c^2 = b_2^2 - a_2^2 = b_1^2 - a_1^2, \quad e_1 = \frac{c}{b_1}, \quad e_2 = \frac{c}{b_2},\\
&\alpha(e) = -\frac{1-e^2}{2e^2} + \frac{\sqrt{1-e^2}}{2e^3}\arcsin(e), \quad \alpha_2 = \alpha(e_2), \quad \alpha_1 = \alpha(e_1),\\
&R_2 = -\frac{a_2 c}{b_2^2} + \arcsin\left(\frac{c}{b_2}\right), \quad Z_2 = \frac{2c}{a_2} - 2\arcsin\left(\frac{c}{b_2}\right),\\
&\chi = \sqrt{\pi^2 + 32/3}, \quad g = \frac{4e_2^3}{3\chi\sqrt{1-e_2^2}}, \quad \tilde{\kappa} = \left(\frac{2}{3} + \frac{g(1-f)(g+2f+gf)}{3(g+1)^2(g+f)^2\ln\frac{g+1}{g+f}}\right)^{-1},\\
&\tilde{sh} = \sinh(2\tilde{\kappa}(\alpha_2 - \alpha_1)), \quad \tilde{ch} = \cosh(2\tilde{\kappa}(\alpha_2 - \alpha_1)),\\
&\eta = \frac{\tilde{\kappa}(1-f)(g+1)(g+f)\tilde{sh}}{(g+1)^2 + (g+f)^2 + 2(g+1)(g+f)(\tilde{\kappa}(\alpha_2-\alpha_1)\tilde{sh} - \tilde{ch})},\\
&C = \frac{(g+1)(g+f)\tilde{\kappa}\tilde{sh}}{(1-f-2\eta(\alpha_2-\alpha_1))\eta}, \quad \overline{F} = \frac{3}{2\tilde{\kappa}}, \quad \overline{H} = \frac{1}{\sqrt{C}}, \quad \overline{G} = \frac{-2\overline{F}\eta}{3\chi g},\\
&\tilde{x}_1 = \frac{c^3}{a_1 b_1^2}, \quad \tilde{x}_2 = \frac{c^3}{a_2 b_2^2}, \quad \tilde{y}_1 = \frac{\chi\tilde{x}_1}{\tilde{x}_1 + 3\chi/4}, \quad \tilde{y}_2 = \frac{\chi\tilde{x}_2}{\tilde{x}_2 + 3\chi/4}, \quad \tilde{f} = \frac{\tilde{y}_2}{\tilde{y}_1}.
\end{aligned} \tag{A.2}$$

and

$$\sigma_0' = \frac{16\pi c^3\sigma_0}{9|\Omega|\tilde{y}_2}.$$

The strain-rate dependent quantities are

$$\mathscr{A} = \frac{\dot{\varepsilon}_{zz} + 2\dot{\varepsilon}_{xx}}{2R_2 + Z_2}, \quad \mathscr{B} = \dot{\varepsilon}_{zz} - \mathscr{A}Z_2, \tag{A.3}$$

where z is the axis of symmetry of the spheroidal voids and (x,y) denote the coordinates in the plane orthogonal to z. The stress being given by derivation of the potential with respect to the strain-rate, one obtains

$$\sigma_{zz} = \frac{\partial \varphi^{\mathrm{GoI}}}{\partial \dot{\varepsilon}_{zz}}(\dot{\varepsilon}_{xx}, \dot{\varepsilon}_{zz}) = n_{\mathrm{sct}}\dot{\varepsilon}_{zz} + 2l_{\mathrm{sct}}\dot{\varepsilon}_{xx},$$

and

$$\sigma_{xx} = \frac{1}{2}\frac{\partial \varphi^{\mathrm{GoI}}}{\partial \dot{\varepsilon}_{xx}}(\dot{\varepsilon}_{xx}, \dot{\varepsilon}_{zz}) = l_{\mathrm{sct}}\dot{\varepsilon}_{zz} + 2\kappa_{\mathrm{sct}}\dot{\varepsilon}_{xx}.$$

The factor 1/2 in the first equality comes from the fact that σ_{xx} is the derivative of φ^{GoI} with respect to $\dot{\varepsilon}_{xx}$ when φ^{GoI} is considered as a function of the three separate variables $\dot{\varepsilon}_{xx}$, $\dot{\varepsilon}_{yy}$ and $\dot{\varepsilon}_{zz}$. However, the expression (A.1) makes use of the equality $\dot{\varepsilon}_{xx} = \dot{\varepsilon}_{yy}$ which leads to a factor 1/2 in the derivation.

The following expressions for the secant moduli are obtained:

$$n_{\mathrm{sct}} = \sigma_0' \int_{\tilde{f}}^1 \left[\frac{\tilde{y}_2^2}{t^2}(\overline{F}\mathscr{A} + \overline{G}\mathscr{B})^2 + \overline{H}^2\mathscr{B}^2\right]^{-1/2}\left[\frac{\tilde{y}_2^2}{t^2}\left(\frac{\overline{F}+2\overline{G}R_2}{2R_2+Z_2}\right)^2 + \left(\frac{2\overline{H}R_2}{2R_2+Z_2}\right)^2\right]\mathrm{d}t \tag{A.4}$$

$$l_{\mathrm{sct}} = \sigma_0' \int_{\tilde{f}}^1 \left[\frac{\tilde{y}_2^2}{t^2}(\overline{F}\mathscr{A} + \overline{G}\mathscr{B})^2 + \overline{H}^2\mathscr{B}^2\right]^{-1/2}\left[\frac{\tilde{y}_2^2}{t^2}\frac{(\overline{F}+2\overline{G}R_2)(\overline{F}-\overline{G}Z_2)}{(2R_2+Z_2)^2} - \frac{2R_2Z_2\overline{H}^2}{(2R_2+Z_2)^2}\right]\mathrm{d}t. \tag{A.5}$$

$$\kappa_{\mathrm{sct}} = \sigma_0' \int_{\tilde{f}}^1 \left[\frac{\tilde{y}_2^2}{t^2}(\overline{F}\mathscr{A} + \overline{G}\mathscr{B})^2 + \overline{H}^2\mathscr{B}^2\right]^{-1/2}\left[\frac{\tilde{y}_2^2}{t^2}\left(\frac{\overline{F}-\overline{G}Z_2}{2R_2+Z_2}\right)^2 + \left(\frac{\overline{H}Z_2}{2R_2+Z_2}\right)^2\right]\mathrm{d}t. \tag{A.6}$$

These secant moduli can be written as functions of $(\dot{\varepsilon}_{zz}^2, \dot{\varepsilon}_{xx}^2, \dot{\varepsilon}_{zz}\dot{\varepsilon}_{xx})$, by noting that

$$\frac{\tilde{y}_2^2}{t^2}(\overline{F}\mathscr{A} + \overline{G}\mathscr{B})^2 + \overline{H}^2\mathscr{B}^2 = \frac{\tilde{y}_2^2}{t^2}(\overline{F}^2\mathscr{A}^2 + \overline{G}^2\mathscr{B}^2 + 2\overline{F}\overline{G}\mathscr{A}\mathscr{B}) + \overline{H}^2\mathscr{B}^2,$$

with

$$\mathscr{A}^2 = \frac{\dot{\varepsilon}_{zz}^2 + 4\dot{\varepsilon}_{xx}^2 + 4\dot{\varepsilon}_{zz}\dot{\varepsilon}_{xx}}{(2R_2+Z_2)^2}, \quad \mathscr{B}^2 = \frac{4R_2^2\dot{\varepsilon}_{zz}^2 + 4Z_2^2\dot{\varepsilon}_{xx}^2 - 8R_2Z_2\dot{\varepsilon}_{zz}\dot{\varepsilon}_{xx}}{(2R_2+Z_2)^2}, \quad \mathscr{A}\mathscr{B} = \frac{2R_2\dot{\varepsilon}_{zz}^2 - 4Z_2\dot{\varepsilon}_{xx}^2 + (4R_2-2Z_2)\dot{\varepsilon}_{zz}\dot{\varepsilon}_{xx}}{(2R_2+Z_2)^2}. \tag{A.7}$$

The secant moduli n_{sct}, l_{sct} and κ_{sct} can be expressed in closed form

$$\begin{aligned}
n_{\mathrm{sct}} &= \sigma_0'\left(\tilde{I}\tilde{y}_2^2\left(\frac{\overline{F}+2\overline{G}R_2}{2R_2+Z_2}\right)^2 + \tilde{J}\left(\frac{2\overline{H}R_2}{2R_2+Z_2}\right)^2\right),\\
l_{\mathrm{sct}} &= \sigma_0'\left(\tilde{I}\tilde{y}_2^2\frac{(\overline{F}+2\overline{G}R_2)(\overline{F}-\overline{G}Z_2)}{(2R_2+Z_2)^2} - \tilde{J}\frac{2R_2Z_2\overline{H}^2}{(2R_2+Z_2)^2}\right),\\
\kappa_{\mathrm{sct}} &= \sigma_0'\left(\tilde{I}\tilde{y}_2^2\left(\frac{\overline{F}-\overline{G}Z_2}{2R_2+Z_2}\right)^2 + \tilde{J}\left(\frac{\overline{H}Z_2}{2R_2+Z_2}\right)^2\right),
\end{aligned} \tag{A.8}$$

with

$$\tilde{I} = \frac{\operatorname{arccsch}\left(\sqrt{\frac{\tilde{b}^2}{\tilde{a}^2}}\tilde{f}\right) - \operatorname{arcsinh}\left(\sqrt{\frac{\tilde{a}^2}{\tilde{b}^2}}\right)}{\sqrt{\tilde{a}^2}}, \quad \tilde{J} = \frac{\sqrt{\tilde{a}^2+\tilde{b}^2} - \sqrt{\tilde{a}^2+\tilde{b}^2\tilde{f}^2}}{\tilde{b}^2},$$

where the function arccsch is the inverse of the hyperbolic cosecant $\operatorname{csch}(x) = 1/\sinh(x)$,

$$\tilde{a}^2 = \tilde{y}_2^2(\overline{F}^2\mathscr{A}^2 + \overline{G}^2\mathscr{B}^2 + 2\overline{F}\overline{G}\mathscr{A}\mathscr{B}), \quad \tilde{b}^2 = \overline{H}^2\mathscr{B}^2.$$

Remark. In the present context, the axis of revolution of the spheroids is the radial direction $\boldsymbol{e}_r$ whereas the in-plane directions x and y are the directions $\boldsymbol{e}_\theta$ and $\boldsymbol{e}_\phi$. Consequently, the above relations are used in Appendix B with $\dot{\varepsilon}_{rr}$ and $\dot{\varepsilon}_{\theta\theta}$ in place of $\dot{\varepsilon}_{zz}$ and $\dot{\varepsilon}_{xx}$, respectively.

Appendix B. Strain field in the linear comparison composite (LCC)

The composite grain occupies a spherical domain Ω with radius R_2. The core of the grain is another spherical domain $\Omega^{(1)}$ with radius R_1 whereas the boundary zone occupies the domain $\Omega^{(2)} = \Omega - \Omega^{(1)}$ such that $R_1 \leqslant r \leqslant R_2$. The volume fraction of the domains are denoted by $f^{(1)}$ and $f^{(2)}$. In this Appendix, both constituents of the composite grain are assumed to be linearly elastic, the central core being isotropic and the outer layer being locally transversally isotropic. The loading consists in an

imposed dilatation on the outer boundary of the grain and to a uniform internal pressure p in the core. For definiteness the detailed solution to this problem is given here. The reader is referred to He and Benveniste, 2004 for a more systematic theory.

The problem to be solved for the LCC reads as

$$\begin{aligned} &\boldsymbol{\sigma} = \mathbf{C}^{(1)} : \boldsymbol{\varepsilon} - p\boldsymbol{i} \quad \text{in } \Omega^{(1)}, \qquad \boldsymbol{\sigma} = \mathbf{C}^{(2)}(\boldsymbol{x}) : \boldsymbol{\varepsilon} \quad \text{in } \Omega^{(2)}, \\ &\operatorname{div}(\boldsymbol{\sigma}) = \mathbf{0} \quad \text{in } \Omega, \qquad \boldsymbol{u} = \boldsymbol{E} \cdot \boldsymbol{x} \quad \text{on } \partial\Omega. \end{aligned} \tag{B.1}$$

The dependence of $\mathbf{C}^{(2)}$ on $\boldsymbol{x}$ stems from the rotation of the local axes of symmetry with the material point $\boldsymbol{x}$ in the outer layer $\Omega^{(2)}$.

B.1. Effective energy

The constitutive relations in (B.1) can formally be written as those of a thermoelastic composite

$$\boldsymbol{\sigma} = \mathbf{C}^{(i)} : \boldsymbol{\varepsilon} + \boldsymbol{\tau}^{(i)}, \quad 1 \leqslant i \leqslant N, \quad \boldsymbol{\tau}^{(1)} = -p\boldsymbol{i}, \quad \boldsymbol{\tau}^{(i)} = \mathbf{0}, \qquad 2 \leqslant i \leqslant N, \tag{B.2}$$

where phase 1 is the central core and the $N-1$ other phases correspond to the different orientations in the outer layer (N is in fact infinite). As in the first part of this study, the effective energy of the LCC can be obtained by a general result about N-phase thermoelastic composites (Willis, 1981) and reads as

$$w^{\text{hom}}(\boldsymbol{E}) = \frac{1}{2}\boldsymbol{E} : \mathbf{C}^{\text{hom}} : \boldsymbol{E} + \boldsymbol{\tau}^{\text{hom}} : \boldsymbol{E} + \frac{1}{2} g^{\text{hom}}, \tag{B.3}$$

with, in particular,

$$\boldsymbol{\tau}^{\text{hom}} = \sum_{i=1}^{N} f^{(i)} \boldsymbol{A}^{(i)^T} : \boldsymbol{\tau}^{(i)}, \qquad g^{\text{hom}} = \sum_{i=1}^{N} f^{(i)} \boldsymbol{\tau}^{(i)} : \boldsymbol{a}^{(i)}. \tag{B.4}$$

In the above relations, $\boldsymbol{A}^{(i)}$ is the (fourth-order) strain-localization tensor which relates the average strain in ith phase to the macroscopic strain $\boldsymbol{E}$ in the absence of eigenstresses ($\boldsymbol{\tau}^{(i)} = 0,\ i = 1, \ldots, N$) and $\boldsymbol{a}^{(i)}$ is the average strain in phase i due to eigenstresses only ($\boldsymbol{E} = \mathbf{0}$). Given that all the $\boldsymbol{\tau}^{(i)}$'s are zero except $\boldsymbol{\tau}^{(1)}$ it is found that the overall elastic energy of the LCC reads as

$$w^{\text{hom}}(\boldsymbol{E}, p) = \frac{1}{2}\boldsymbol{E} : \mathbf{C}^{\text{hom}} : \boldsymbol{E} - p\boldsymbol{B}^{\text{hom}} : \boldsymbol{E} - \frac{1}{2}\frac{p^2}{M^{\text{hom}}} \tag{B.5}$$

with

$$\boldsymbol{B}^{\text{hom}} = f^{(1)}\boldsymbol{i} : \boldsymbol{A}^{(1)}, \qquad \frac{1}{M^{\text{hom}}} = \frac{f^{(1)}}{p}\boldsymbol{i} : \boldsymbol{a}^{(1)}. \tag{B.6}$$

The effective relation between the overall stress and the overall strain is obtained by derivation of (B.5)

$$\boldsymbol{\Sigma} = \mathbf{C}^{\text{hom}} : \boldsymbol{E} - p\boldsymbol{B}^{\text{hom}}. \tag{B.7}$$

To simplify further this relation it is noted that the stress $\boldsymbol{\Sigma}$ and the average strain in the core $\boldsymbol{a}^{(1)}$ generated by the sole application of a pressure p in the core of the grain (with $\boldsymbol{E} = \mathbf{0}$) are purely hydrostatic by spherical symmetry. It follows that $\boldsymbol{B}^{\text{hom}}$ (proportional to $\boldsymbol{\Sigma}$ when $\boldsymbol{E} = \mathbf{0}$) and $\boldsymbol{a}^{(1)}$ are proportional to $\boldsymbol{i}$:

$$\boldsymbol{B}^{\text{hom}} = b^{\text{hom}}\boldsymbol{i}, \quad b^{\text{hom}} = \frac{1}{3}\boldsymbol{B}^{\text{hom}} : \boldsymbol{i} = \frac{f^{(1)}}{3}\boldsymbol{i} : \boldsymbol{A}^{(1)} : \boldsymbol{i}, \quad \boldsymbol{a}^{(1)} = a^{(1)}\boldsymbol{i}, \quad a^{(1)} = \frac{1}{3}\boldsymbol{a}^{(1)} : \boldsymbol{i}. \tag{B.8}$$

Similarly, when the composite grain is subjected to a hydrostatic deformation $E_m\boldsymbol{i}$ only, the response of the composite grain is again hydrostatic and proportional to E_m. The ratio $k^{\text{hom}} = \Sigma_m / 3E_m$ is the effective bulk modulus of the composite grain. Finally, when the composite grain is subjected to both an internal pressure p in the core and an average deformation $E_m\boldsymbol{i}$, the overall stress is hydrostatic with

$$\Sigma_m = 3k^{\text{hom}}E_m - pb^{\text{hom}},$$

and the effective energy reads as

$$w^{\text{hom}}(E_m, p) = \frac{9k^{\text{hom}}}{2}E_m^2 - 3pb^{\text{hom}}E_m - \frac{1}{2}\frac{p^2}{M^{\text{hom}}}. \tag{B.9}$$

Thanks to the relation (B.8), it is sufficient to solve the purely elastic problem ($E_m \neq 0,\ p = 0$) to determine both the effective modulus b^{hom} and the effective bulk modulus k^{hom} (see Section B.2). The effective Biot modulus M^{hom} is obtained by means of the last relation in (B.6) and the determination of $\boldsymbol{a}^{(1)}$ requires the resolution of the local problem (B.1) with $p \neq 0, E_m = 0$ (see Section B.3).

B.2. Response of the composite grain under a purely hydrostatic deformation

In this section, the grain is drained ($p = 0$) and subjected to an imposed dilatation on its boundary

$$\boldsymbol{u} = E_m \boldsymbol{I} \cdot \boldsymbol{x} \quad \text{on } \partial\Omega. \tag{B.10}$$

The objective of this section is to derive an explicit expression for the displacement field in the composite grain and to use this expression to determine the effective bulk modulus k^{hom} of the composite grain and the scalar coefficient b^{hom}.

The displacement field is radial in Ω and depends on r only (where (r, θ, ϕ) denote classically the spherical coordinates) $\boldsymbol{u} = u(r)\boldsymbol{e}_r$. The strain tensor is diagonal in the spherical frame

$$\varepsilon_{rr} = \frac{\partial u}{\partial r}, \quad \varepsilon_{\theta\theta} = \varepsilon_{\phi\phi} = \frac{u}{r}. \tag{B.11}$$

The notations of Walpole, 1969 will be used to describe the transversely isotropic elasticity of the outer layer $\Omega^{(2)}$. When the strain is axisymmetric, the constitutive relations in the layer can be expressed with the help of three elastic coefficients in the form

$$\sigma_{rr} = n\varepsilon_{rr} + 2l\varepsilon_{\theta\theta}, \quad \sigma_{\theta\theta} = l\varepsilon_{rr} + 2\kappa\varepsilon_{\theta\theta}. \tag{B.12}$$

Similar constitutive relations hold in the core, except that due to the isotropy of the core material, the three elastic coefficients (n, l, κ) in the core depend on two elastic constants, the bulk and shear moduli k and μ of the core

$$n = k + \frac{4}{3}\mu, \quad l = k - \frac{2}{3}\mu, \quad \kappa = \frac{1}{3}(3k + \mu) \text{ in the core}. \tag{B.13}$$

The equilibrium equation along the radial direction

$$\frac{\partial \sigma_{rr}}{\partial r} + \frac{2(\sigma_{rr} - \sigma_{\theta\theta})}{r} = 0$$

combined with the expression (B.11) of the strain field gives a differential equation for the displacement field

$$n\frac{\partial^2 u}{\partial r^2} + \frac{2n}{r}\frac{\partial u}{\partial r} + 2(l - 2\kappa)\frac{u}{r^2} = 0, \tag{B.14}$$

the solution of which is (separately in $\Omega^{(1)}$ and $\Omega^{(2)}$)

$$u(r) = Ar^{\alpha} + Br^{\beta} \quad \text{with } \alpha = \frac{-n + \sqrt{n^2 - 8n(l - 2\kappa)}}{2n}, \quad \beta = \frac{-n - \sqrt{n^2 - 8n(l - 2\kappa)}}{2n}. \tag{B.15}$$

The exponents (α, β) and the constants (A, B) are different in the core and in the outer layer.

In the isotropic core, it is well known (and readily checked) that $\alpha = 1$ and $\beta = -2$. In order to avoid a singularity of the displacement field in r^{-2} at $r = 0, B = 0$ and the displacement field in the core is simply $u(r) = Ar$. The strain and the stress in the core are hydrostatic:

$$\varepsilon_{rr} = \varepsilon_{\theta\theta} = \varepsilon_{\phi\phi} = A, \quad \sigma_{rr} = \sigma_{\theta\theta} = \sigma_{\phi\phi} = 3kA. \tag{B.16}$$

In order to avoid confusion, we will now label the elastic coefficients and the unknowns by the phase. The elastic coefficients are $k^{(1)}$ in the core and $(n^{(2)}, l^{(2)}, \kappa^{(2)})$ in the outer layer. The exponents α and β in the outer layer are given by the relations (B.15) with $(n^{(2)}, l^{(2)}, \kappa^{(2)})$. We are left with three unknowns $A^{(1)}$ (in the core) and $(A^{(2)}, B^{(2)})$ in the outer layer which solve three equations expressing the continuity of u and σ_{rr} at the interface $r = R_1$ and the imposed displacement at $r = R_2$ (E_m is taken equal to 1 by homogeneity):

$$\begin{aligned}
&A^{(2)}R_1^{\alpha} + B^{(2)}R_1^{\beta} = A^{(1)}R_1, \\
&(n^{(2)}\alpha + 2l^{(2)})A^{(2)}R_1^{\alpha-1} + (n^{(2)}\beta + 2l^{(2)})B^{(2)}R_1^{\beta-1} = 3k^{(1)}A^{(1)}, \\
&A^{(2)}R_2^{\alpha} + B^{(2)}R_2^{\beta} = R_2.
\end{aligned} \tag{B.17}$$

A straightforward calculation leads to

$$A^{(1)} = f^{(1)^{\frac{\beta-1}{3}}}\Delta + f^{(1)^{\frac{\alpha-1}{3}}}(1 - \Delta), \quad A^{(2)} = R_2^{1-\alpha}(1 - \Delta), B^{(2)} = R_2^{1-\beta}\Delta \tag{B.18}$$

with

$$\Delta = \left[1 - f^{(1)^{\frac{\beta-\alpha}{3}}}\frac{3k^{(1)} - n^{(2)}\beta - 2l^{(2)}}{3k^{(1)} - n^{(2)}\alpha - 2l^{(2)}}\right]^{-1}.$$

The first moments of the strain field in the phases are given by

$$\langle \varepsilon_{rr} \rangle_1 = \langle \varepsilon_{\theta\theta} \rangle_1 = A^{(1)}, \tag{B.19}$$

$$\langle \varepsilon_{rr}\rangle_2 = \frac{4\pi}{|\,\Omega^{(2)}\,|}\int_{R_1}^{R_2}\frac{\partial u}{\partial r}(r)r^2\,\mathrm{d}r = \frac{3}{f^{(2)}}\left[\frac{\alpha}{\alpha+2}A^{(2)}R_2^{\alpha-1}(1-f^{(1)^{\frac{\alpha+2}{3}}}) + \frac{\beta}{\beta+2}B^{(2)}R_2^{\beta-1}\left(1-f^{(1)^{\frac{\beta+2}{3}}}\right)\right], \tag{B.20}$$

$$\langle \varepsilon_{\theta\theta}\rangle_2 = \frac{4\pi}{|\,\Omega^{(2)}\,|}\int_{R_1}^{R_2}\frac{u(r)}{r}r^2\,\mathrm{d}r = \frac{3}{f^{(2)}}\left[\frac{1}{\alpha+2}A^{(2)}R_2^{\alpha-1}\left(1-f^{(1)^{\frac{\alpha+2}{3}}}\right) + \frac{1}{\beta+2}B^{(2)}R_2^{\beta-1}\left(1-f^{(1)^{\frac{\beta+2}{3}}}\right)\right], \tag{B.21}$$

It is easily deduced from the relations (B.18)–(B.21) that

$$\langle \varepsilon_m\rangle_1 = \frac{1}{3}\langle \varepsilon_{rr}+2\varepsilon_{\theta\theta}\rangle_1 = C_E^{(1)}, \quad \langle \varepsilon_m\rangle_2 = \frac{1}{3}\langle \varepsilon_{rr}+2\varepsilon_{\theta\theta}\rangle_2 = C_E^{(2)}, \quad \frac{1}{3}\langle \varepsilon_{rr}-\varepsilon_{\theta\theta}\rangle_2 = D_E^{(2)} \tag{B.22}$$

with

$$\begin{aligned} C_E^{(1)} &= f^{(1)^{\frac{\beta-1}{3}}}\Delta + f^{(1)^{\frac{\alpha-1}{3}}}(1-\Delta),\\ C_E^{(2)} &= \frac{1}{f^{(2)}}\left[(1-\Delta)\left(1-f^{(1)^{\frac{\alpha+2}{3}}}\right)+\Delta\left(1-f^{(1)^{\frac{\beta+2}{3}}}\right)\right],\\ D_E^{(2)} &= \frac{1}{f^{(2)}}\left[\frac{\alpha-1}{\alpha+2}(1-\Delta)\left(1-f^{(1)^{\frac{\alpha+2}{3}}}\right)+\frac{\beta-1}{\beta+2}\Delta\left(1-f^{(1)^{\frac{\beta+2}{3}}}\right)\right]. \end{aligned} \tag{B.23}$$

The overall bulk modulus k^{hom} follows directly from the expression of the overall stress (recall that $E_m = 1$), $3k^{\mathrm{hom}} = \Sigma_m = f^{(1)}\langle\sigma_m\rangle_1 + f^{(2)}\langle\sigma_m\rangle_2$:

$$3k^{\mathrm{hom}} = 3k^{(1)}f^{(1)}\langle\varepsilon_m\rangle_1 + \frac{(n^{(2)}+2l^{(2)})}{3}f^{(2)}\langle\varepsilon_{rr}\rangle_2 + \frac{(2l^{(2)}+4\kappa^{(2)})}{3}f^{(2)}\langle\varepsilon_{\theta\theta}\rangle_2.$$

This expression can be simplified by noting that

$$1 = E_m = f^{(1)}\langle\varepsilon_m\rangle_1 + f^{(2)}\langle\varepsilon_m\rangle_2, \quad \langle\varepsilon_{rr}\rangle_2 = \langle\varepsilon_m\rangle_2 + \frac{2}{3}\langle\varepsilon_{rr}-\varepsilon_{\theta\theta}\rangle_2, \quad \langle\varepsilon_{\theta\theta}\rangle_2 = \langle\varepsilon_m\rangle_2 - \frac{1}{3}\langle\varepsilon_{rr}-\varepsilon_{\theta\theta}\rangle_2$$

into

$$\Sigma_m = 3k^{(1)}(E_m - f^{(2)}\langle\varepsilon_m\rangle_2) + \frac{(n^{(2)}+4l^{(2)}+4\kappa^{(2)})}{3}f^{(2)}\langle\varepsilon_m\rangle_2 + \frac{2(n^{(2)}+l^{(2)}-2\kappa^{(2)})}{9}f^{(2)}\langle\varepsilon_{rr}-\varepsilon_{\theta\theta}\rangle_2.$$

The final expression of the effective bulk modulus is obtained with the help of the relations (B.22)

$$\begin{aligned} k^{\mathrm{hom}} = k^{(1)} &+ \left(\frac{(n^{(2)}+4l^{(2)}+4\kappa^{(2)})}{9} - k^{(1)}\right)\left[(1-\Delta)\left(1-f^{(1)^{\frac{\alpha+2}{3}}}\right)+\Delta\left(1-f^{(1)^{\frac{\beta+2}{3}}}\right)\right]\\ &+ \frac{2(n^{(2)}+l^{(2)}-2\kappa^{(2)})}{9}\left[\frac{\alpha-1}{\alpha+2}(1-\Delta)\left(1-f^{(1)^{\frac{\alpha+2}{3}}}\right)+\frac{\beta-1}{\beta+2}\Delta(1-f^{(1)^{\frac{\beta+2}{3}}})\right]. \end{aligned} \tag{B.24}$$

The scalar b^{hom} entering (B.8) is related to $A^{(1)}$ given by the first relation in (B.18) by

$$b^{\mathrm{hom}} = f^{(1)}A^{(1)}. \tag{B.25}$$

B.3. Response of the composite grain under a pressure in the core only

The problem is now (B.1) where $p\neq 0$, $\boldsymbol{E} = 0$. The displacement field in the two phases is still in the form (B.15) with three unknowns $A^{(1)}, A^{(2)}, B^{(2)}$ which solve the algebraic system of equations

$$\begin{aligned} &A^{(2)}R_1^{\alpha} + B^{(2)}R_1^{\beta} = A^{(1)}R_1,\\ &(n^{(2)}\alpha + 2l^{(2)})A^{(2)}R_1^{\alpha-1} + (n^{(2)}\beta + 2l^{(2)})B^{(2)}R_1^{\beta-1} = 3k^{(1)}A^{(1)} - p,\\ &A^{(2)}R_2^{\alpha} + B^{(2)}R_2^{\beta} = 0. \end{aligned} \tag{B.26}$$

Taking $p = 1$ by homogeneity, a straightforward calculation leads to

$$A^{(1)} = \left(f^{(1)^{\frac{\alpha-1}{3}}} - f^{(1)^{\frac{\beta-1}{3}}}\right)\Gamma, \quad A^{(2)} = R_2^{1-\alpha}\Gamma, \quad B^{(2)} = -R_2^{1-\beta}\Gamma \tag{B.27}$$

with

$$\Gamma = \frac{1}{(3k^{(1)} - n^{(2)}\alpha - 2l^{(2)})f^{(1)^{\frac{\alpha-1}{3}}} - (3k^{(1)} - n^{(2)}\beta - 2l^{(2)})f^{(1)^{\frac{\beta-1}{3}}}}.$$

Finally, the scalar $a^{(1)}$ entering (B.8) is $pA^{(1)}$, where $A^{(1)}$ given by the first relation in (B.27), from which it is deduced that

$$\frac{1}{M^{\hom}} = 3\left(f^{(1)\frac{\alpha+2}{3}} - f^{(1)\frac{\beta+2}{3}}\right)\Gamma.$$

The first moments in the phases of the components of the strain are still given by the general relations (B.19)–(B.21). We obtain in particular that

$$\langle \varepsilon_m \rangle_1 = \frac{1}{3}\langle \varepsilon_{rr} + 2\varepsilon_{\theta\theta} \rangle_1 = C_p^{(1)}, \quad \langle \varepsilon_m \rangle_2 = \frac{1}{3}\langle \varepsilon_{rr} + 2\varepsilon_{\theta\theta} \rangle_2 = C_p^{(2)}, \quad \frac{1}{3}\langle \varepsilon_{rr} - \varepsilon_{\theta\theta} \rangle_2 = D_p^{(2)}$$

with

$$\begin{aligned} C_p^{(1)} &= \left(f^{(1)\frac{\alpha-1}{3}} - f^{(1)\frac{\beta-1}{3}}\right)\Gamma, \quad C_p^{(2)} = \frac{1}{f^{(2)}}\left(f^{(1)\frac{\beta+2}{3}} - f^{(1)\frac{\alpha+2}{3}}\right)\Gamma \\ D_p^{(2)} &= \frac{1}{f^{(2)}}\Gamma\left[\frac{\alpha-1}{\alpha+2}\left(1 - f^{(1)\frac{\alpha+2}{3}}\right) - \frac{\beta-1}{\beta+2}\left(1 - f^{(1)\frac{\beta+2}{3}}\right)\right]. \end{aligned} \tag{B.28}$$

B.4. First moments of the strain field in the phase under general loading conditions $E_m \neq 0, p \neq 0$

Under general loading conditions, $E_m \neq 0, p \neq 0$, the first moments of the strain field in the phases which will be useful in the evolution equation (28)–(30) read as

$$\langle \varepsilon_m \rangle_1 = C_E^{(1)} E_m + C_p^{(1)} p, \quad \langle \varepsilon_m \rangle_2 = C_E^{(2)} E_m + C_p^{(2)} p, \quad \frac{1}{3}\langle \varepsilon_{rr} - \varepsilon_{\theta\theta} \rangle_2 = D_E^{(2)} E_m + D_p^{(2)} p. \tag{B.29}$$

References

Benzerga, A., 2002. Micromechanics of coalescence in ductile fracture. J. Mech. Phys. Solids 50, 1331–1362.

Fabrègue, D., Pardoen, T., 2008. A constitutive model for elastoplastic solids containing primary and secondary voids. J. Mech. Phys. Solids 56, 719–741.

Gologanu, M., Leblond, J., Devaux, J., 1994. Approximate models for ductile metals containing non-spherical voids-case of axisymmetric oblate ellipsoidal cavities. ASME J. Eng. Mater. Technol. 116, 290–297.

Gurson, A., 1977. Continuum theory of ductile rupture by void nucleation and growth: Part I – yield criteria and flow rules for porous ductile media. J. Eng. Mater. Technol. 99, 1–15.

He, Q., Benveniste, Y., 2004. Exactly solvable spherically anisotropic thermoelastic microstructures. J. Mech. Phys. Solids 52, 2661–2682.

Koplik, J., Needleman, A., 1988. Void growth and coalescence in porous plastic solids. Int. J. Solids Struct. 24, 835–853.

Nguyen, Q., 1977. On the elastic–plastic initial boundary value problem and its numerical integration. Int. J. Numer. Meth. Eng. 11, 817–832.

Pardoen, T., Dumont, D., Deschamps, A., Brechet, Y., 2003. Grain boundary versus transgranular ductile failure. J. Mech. Phys. Solids 51, 637–665.

Pardoen, T., Hutchinson, J., 2000. An extended model for void growth and coalescence. J. Mech. Phys. Solids 48, 2467–2512.

Pardoen, T., Hutchinson, J., 2003. Micromechanics-based model for trends in toughness of ductile metals. Acta Mater. 51, 133–148.

Ponte Castañeda, P., 1991. The effective mechanical properties of nonlinear isotropic composites. J. Mech. Phys. Solids 39, 45–71.

Ponte Castañeda, P., Zaidman, M., 1996. The finite deformation of nonlinear composite materials. i. Instantaneous constitutive relations. Int. J. Solids Struct. 33, 1271–1286.

Simo, J., Hughes, T., 1998. Computational Inelasticity. Interdisciplinary Applied Mathematics, vol. 7. Springer, New York.

Thomason, P., 1985. Three-dimensional models for the plastic limit-loads at incipient failure of the intervoid matrix in ductile porous solids. Acta Metall. 33 (6), 1079–1085.

Vincent, P., Monerie, Y., Suquet, P., 2008. Porous materials with two populations of voids under internal pressure: I instantaneous constitutive relations. Int. J. Solids Struct.

Walpole, L., 1969. On the overall elastic moduli of composite materials. J. Mech. Phys. Solids 17, 235–251.

Willis, J., 1981. Variational and related methods for the overall properties of composites. In: Yih, C. (Ed.), Advances in Applied Mechanics, vol. 21. Academic Press, New York, pp. 1–78.